

Journal Pre-proof

Microdialysis probes and digital twins reveal the rapid removal of fertiliser phosphate from the soil solution with an impact on crop nutrition in the short-term

C. Petroselli, K.A. Williams, S.A. Ruiz, D. McKay Fletcher, M.J. Cooper, T. Roose



PII: S0038-0717(24)00106-8

DOI: <https://doi.org/10.1016/j.soilbio.2024.109417>

Reference: SBB 109417

To appear in: *Soil Biology and Biochemistry*

Received Date: 30 October 2023

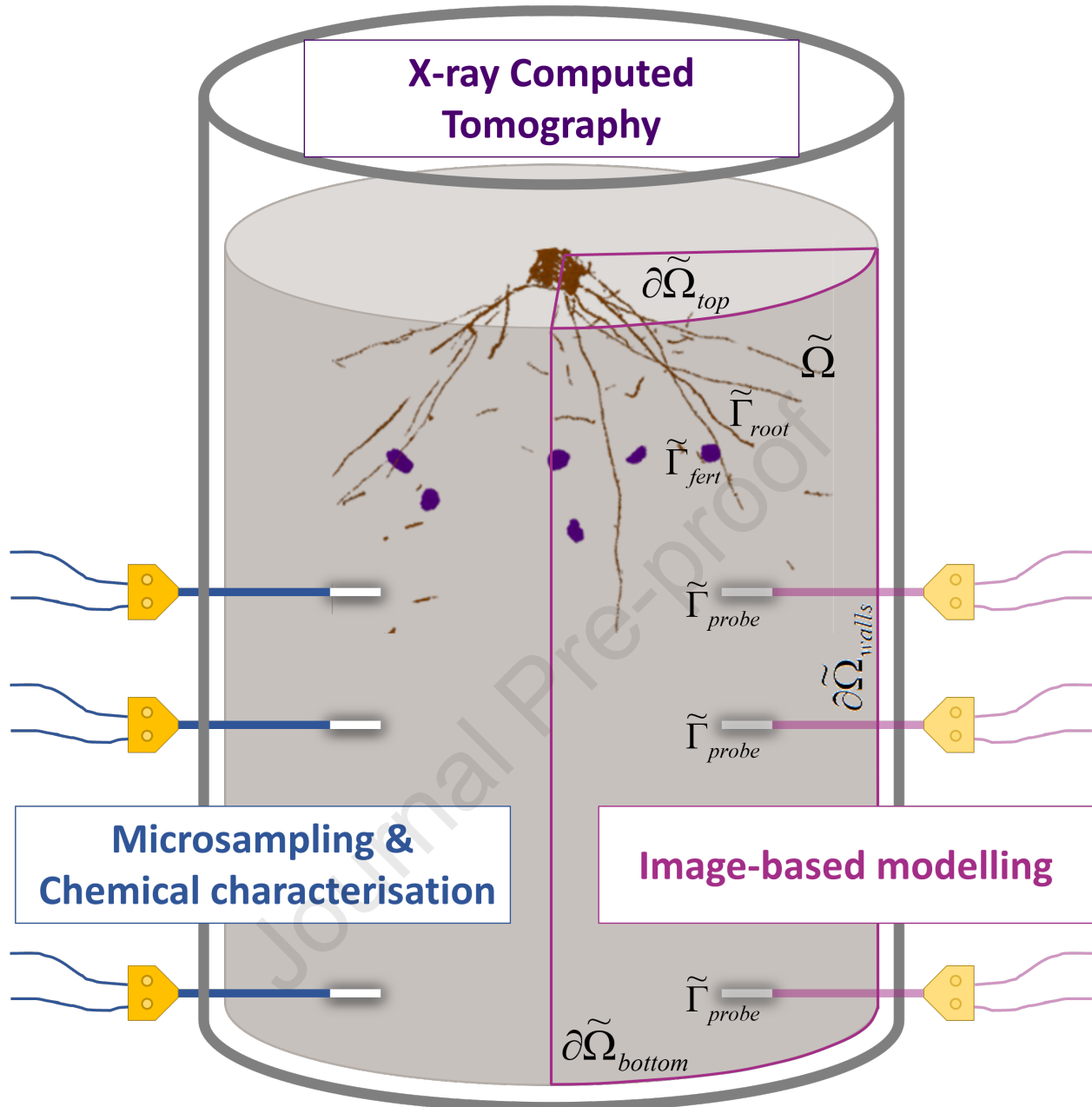
Revised Date: 19 March 2024

Accepted Date: 26 March 2024

Please cite this article as: Petroselli, C., Williams, K.A., Ruiz, S.A., McKay Fletcher, D., Cooper, M.J., Roose, T., Microdialysis probes and digital twins reveal the rapid removal of fertiliser phosphate from the soil solution with an impact on crop nutrition in the short-term, *Soil Biology and Biochemistry* (2024), doi: <https://doi.org/10.1016/j.soilbio.2024.109417>.

This is a PDF file of an article that has undergone enhancements after acceptance, such as the addition of a cover page and metadata, and formatting for readability, but it is not yet the definitive version of record. This version will undergo additional copyediting, typesetting and review before it is published in its final form, but we are providing this version to give early visibility of the article. Please note that, during the production process, errors may be discovered which could affect the content, and all legal disclaimers that apply to the journal pertain.

© 2024 Published by Elsevier Ltd.



1 Microdialysis probes and digital twins
2 reveal the rapid removal of fertiliser
3 phosphate from the soil solution with an
4 impact on crop nutrition in the short-
5 term

C. Petroselli^{1,2,+}, K. A. Williams^{1,3,+}, S. A. Ruiz^{1,+}, D. McKay Fletcher^{1,5,+}, M.J. Cooper⁴, T. Roose^{1,*}

¹University of Southampton, School of Engineering, Faculty of Engineering and Physical Sciences, Southampton (UK)

²University of Perugia, Department of Chemistry, Biology and Biotechnology, Perugia (Italy)

³University of Portsmouth, Faculty of Science and Health, Portsmouth (UK)

⁴University of Southampton, National Oceanography Centre, Southampton (UK)

⁵Scotlands Rural College, Rural Economy, Environment and Society Research Group, Edinburgh (UK)

⁺Denotes equal contribution by authors

^{*}Denotes corresponding author: t.roose@soton.ac.uk, School of Engineering, Faculty of Engineering and Physical Sciences, University of Southampton, University Road, Southampton SO17 1BJ, United Kingdom

6 Abstract

7 Global food production depends on the application of phosphorus (P) fertilisers, usually sourced from
8 rock phosphate, a non-renewable resource. Optimising P use to ensure sustainable P application is
9 necessary to supply food worldwide and to protect the environment from P runoff. However, standard
10 models used to guide P application on fields are limited due to assumptions that fail to consider the
11 short-term dynamics of P in the soil solution. This study combined time-resolved microdialysis

12 sampling with 4D spatial information from X-ray computed tomography to inform an image-based
13 model for assessing P-soil-plant interactions over the start of a growing season. The time-resolved
14 microdialysis measurements revealed that P released from the granules is rapidly removed from the
15 soil solution in the short-term. We demonstrate that the standard equilibrium models typically used
16 to characterise P transport in soil are not representative of the experimental system on the time scales
17 considered. Instead, an Absorption-Diffusion model, where a single sink term accounts for all the
18 processes removing P from the soil solution was required to correctly characterise experimental
19 observations. Our study provides the basis for a model which could be adapted to predict within-
20 season fertilisation scenarios in different soil conditions, and provides a conceptual description of
21 plant/crop yield response to P fertilisation.

22 Keywords:

23 Phosphorus, Microdialysis, X-ray Computed Tomography, Image-based modelling, Precision
24 agriculture

25 1. Introduction

26 Phosphorus (P) is an essential plant nutrient, and one that is often yield-limiting in agricultural
27 systems. Thus, P availability to crop plants is vital for productive agriculture and efficient land use
28 (Barber, 1995). Global demand for P fertiliser has increased with growing human population (Cordell
29 et al., 2009) and P-fertiliser prices increased from 120 to 320 EUR per metric ton in the last year (2022;
30 (Mundi, 2022)). Soil P stocks and access to P fertilisers are not equally distributed around the world.
31 One in five children worldwide are affected by malnourishment linked to fertiliser (*i.e.* P) scarcity
32 (Kahiluoto et al., 2021), but in much of Western Europe, the USA and China, agricultural soils show
33 high total P content due to over fertilisation in 20th century (also called legacy P). Phosphorus
34 accumulation in the EU and the US soils ranges from 700-800 kg ha⁻¹ and 230-1400 kg ha⁻¹, respectively
35 (Kahiluoto et al., 2021). In some cases, ceasing the application of P fertiliser would not have an adverse
36 effect on yield for several years (Valkama et al., 2011; Sattari et al., 2012; Sattari et al., 2014). In
37 developed nations, farmers are hypothesised to keep the soil P levels high as insurance against P
38 deficiency limiting yields and to use the soil as a 'bank' to protect against increases in future P fertiliser
39 prices (Macintosh et al., 2019). However, in sub-Saharan Africa and less developed sub-tropical
40 country agricultural soils, insufficient P input limits yields (Nziguheba et al., 2016). Phosphorus deficits
41 in developing countries are on the order of 125-250 kg ha⁻¹ affecting ~200-300 Mha of arable land area
42 (Kahiluoto et al., 2021).

43 Together, the over application of P in some regions, depletion of P in others, and a looming P supply
44 crisis require efforts to optimise P use efficiency on the global scale, on the scale of individual fields
45 and even on individual fertiliser granule scale. One approach to tackling P use efficiency is to optimise
46 the within-season use of P fertiliser using precision agriculture approaches (Cisternas et al., 2020; Ros
47 et al., 2020); this requires an understanding of the fundamental processes underlying short timescale
48 P dynamics and uptake in soil. Low Soil Test Phosphorus (low-STP) soils typically have a larger yield
49 response to P fertilisation than high-STP soils (Ros et al., 2020). However, it remains unclear as to
50 when farmers can expect larger yield responses. Some of these uncertainties can be attributed to
51 theoretical assumptions based on long term observations that may not be valid in low-STP soils at
52 shorter timescales.

53 Phosphorus fertilisation usually includes the application of P as soluble compounds that release
54 phosphate into the soil solution where plant roots can directly access it (Hedley and McLaughlin,
55 2005). The application of P soluble compounds generates a sharp increase in P soil solution
56 concentration, which favours the plant uptake, but could also result in P leaching and runoff leading
57 to pollution and eutrophication of water bodies (Cornish, 2009). It is well known that most of the
58 supplied P (about 70%) is not taken up by plants in the first harvest, but it is retained in the soil
59 (Barrow, 1980) and is thought to keep sustaining the crops as a long-term P-legacy, even though its
60 efficiency greatly decreases over time (Bolland and Gilkes, 1998). However, the understanding of
61 intra-seasonal short-term dynamics of P in the soil solution, that could shed light on how to maximise
62 the effect of the supplied P on crops while reducing runoff, is less well understood as high frequency
63 time-resolved techniques are (Demand et al., 2017; Gao et al., 2019a; Petroselli et al., 2021).
64 Phosphorus concentration in the soil solution decreases after fertiliser application mainly due to
65 sorption, i.e., adsorption onto soil particles surfaces followed by possible absorption inside the soil
66 solids structure (Barrow, 1983) and precipitation of secondary P-rich phases driven by oversaturation
67 or favoured by sorption (Pierzynski et al., 2005). Moreover, microbially mediated immobilisation (i.e.
68 conversion of inorganic P into organic P) and the opposite process, mineralisation, also have an
69 important effect in the P cycle in natural soils (Condon et al., 2005). In this paper, we are going to
70 refer to retained-P as the fraction of P that is removed from the soil solution due to the combined
71 effect of all the aforementioned processes, i.e., the P that is not immediately available to plants in soil
72 solution. Typically, the proportion of retained-P to solution-P is between 40-1000 (Barber, 1995) and
73 the concentration of P in the soil solution is $<10 \mu\text{M}$ (Schachtman et al., 1998). Therefore, the
74 availability of P to plants depends on how quickly P is removed from the soil solution due to sorption,
75 precipitation, immobilisation and microbial uptake. While certain mathematical models consider
76 explicit reactions and rates of binding (Barrow, 1974), they are often limited to bulk estimation of

77 parameter values that do not resolve spatial or even temporal small scale distributions of P. The typical
78 theoretical model invoked to resolve transport of P and spatial distributions in soil relies on
79 equilibrium reaction assumptions. In particular, the ratio between solution-P and retained-P is
80 considered to be immediately in equilibrium based on the assumption that these reactions occur at
81 rates more rapid than the rates of transport through soil (*i.e.* diffusion) (Barber, 1995). Under this
82 model assumption, the P repeatedly binds and dissolves again from the soil surface, which slows its
83 net rate of transport, leading to effective slow diffusion of P through soil. While this model is
84 appropriate for large field sites or ecosystems over long time scales to describe dynamics of legacy-P,
85 it cannot account for short-term local processes. For example, a recent study demonstrated that in
86 small scale experiments low soil test P soils acted as sinks for even relatively large fertiliser applications
87 (Petroselli et al. (2021)). Quantities of P fertiliser in excess of those applied to farm fields were found
88 to be rapidly removed from the soil solution and were not measured again in solution after a 2-week
89 period. While the P sorption and desorption almost certainly reaches an equilibrium, in this study the
90 measured desorption from the soil was negligible. Petroselli et al. (2021) also observed rapid transport
91 of P up to distances of 3 cm from the fertiliser granule, which, while being coherent with previous
92 observations (Benbi and Gilkes, 1987), is not reproduced by the standard equilibrium mathematical
93 model, which predicts a significant impedance to diffusive fluxes. In other words, the assumptions of
94 a standard equilibrium model are not compatible with experimental results at small time and space
95 scales. These results highlight a limitation to the standard equilibrium reaction assumption on intra-
96 seasonal plant scale processes and suggest the need for an alternative dynamic modelling approach
97 for low-STP soils. This has implications for field-scale predictions, because if P exists in the soil solution
98 only for a narrow period of time (as suggested by rapid removal from soil solution), the timing of
99 fertiliser application with respect to weather patterns and crop demand is crucial to get the most yield
100 from the concentrated soil solution. However, gaining sufficient understanding of the dynamics of P
101 in the soil solution at high temporal and spatial resolution requires time- and space-resolved
102 experimental measurements of P concentrations.

103 This spatiotemporal approach is challenging, however, state of the art micro-sampling techniques,
104 including suction cups and microdialysis probes, are helping to elucidate the underpinning processes
105 that mediate P-dynamics in soil. Although these probes were originally designed for pharmacokinetics
106 (Hammarlund-Udenaes, 2017; Petroselli et al., 2021), they can be used to sample the soil solution *in*
107 *situ* and gain time resolved data on soil solution concentrations (Gao et al., 2019b; Petroselli et al.,
108 2021). Microdialysis probe solute measurements have been used less frequently, but they have an
109 advantage over suction cups as the measurements rely on passive diffusion of P across a semi-
110 permeable membrane thus not affecting soil water transport. Moreover, microdialysis probes mimic

111 root solute uptake from the soil solution, and have therefore been used as artificial roots (McKay
112 Fletcher et al., 2019; Buckley et al., 2020; König et al., 2022).

113 Time resolved *in situ* chemical sampling is a powerful technique in itself, but its coupling with time-
114 resolved 3D imaging of exact experimental setups and plant root structures enables to develop an
115 image-based, 3D, spatially and temporally explicit model, which can act as a digital twin of the
116 experimental system. Previous studies have demonstrated the utility of X-ray computed tomography
117 (XCT) imaging as a tool for assessing spatial trends associated with plant development under varying
118 fertilisation treatments (Ahmed et al., 2016). For example, morphometric features in these imaging
119 studies were able to assess that root system architecture was broader in soils without fertilisation vs
120 those with fertiliser granules, indicating plants employ an 'exploration strategy' under low-STP
121 conditions (Williams et al., 2022). Furthermore, the present study used the XCT images to generate
122 mathematical models, which extended the utility of the imaging. The models were able to make
123 predictions about soil solution P concentrations, transport, and root P acquisition (Williams et al.,
124 2022). Using this information, the model was able to predict optimal fertilisation strategies based on
125 P availability in the soil solution and general soil buffering.

126 The current study builds on the aforementioned results by combining time resolved microdialysis
127 sampling, XCT measurements, and image based modelling. Specifically, the study:

- 128 • Develops an experimental set up considering growing wheat plants in pots under different
129 fertilisation regimes (early, late, and no P fertilisation);
- 130 • Measures soil solution P dynamics using high frequency microdialysis sampling at varying
131 depths along the pot;
- 132 • Monitors root system development using time lapsed XCT imaging for the different
133 treatments;
- 134 • Assess the suitability of two different image-based modelling approaches for simulating the
135 experimental results;
- 136 • Develops an inverse modelling protocol to match the model results to the microdialysis
137 measurements.

138 Our aim is to quantify soil solution P dynamics in a low-STP soil, compare the efficiency of different
139 fertilisation protocols with different timings relative to plant root growth, and test if the dynamics of
140 plant available P can be replicated using two different models: The buffer power model which assumes
141 that the soil-P reactions are in equilibrium resulting in impeded diffusion; and the Absorption-
142 Diffusion model which considers the removal of solute (e.g. surface binding, aggregate trapped,

143 microbial activity) from the soil solution to be the dominant reactive process governing P transport
144 and root uptake.

145 2. Materials and Methods

146 2.1 Experimental set up

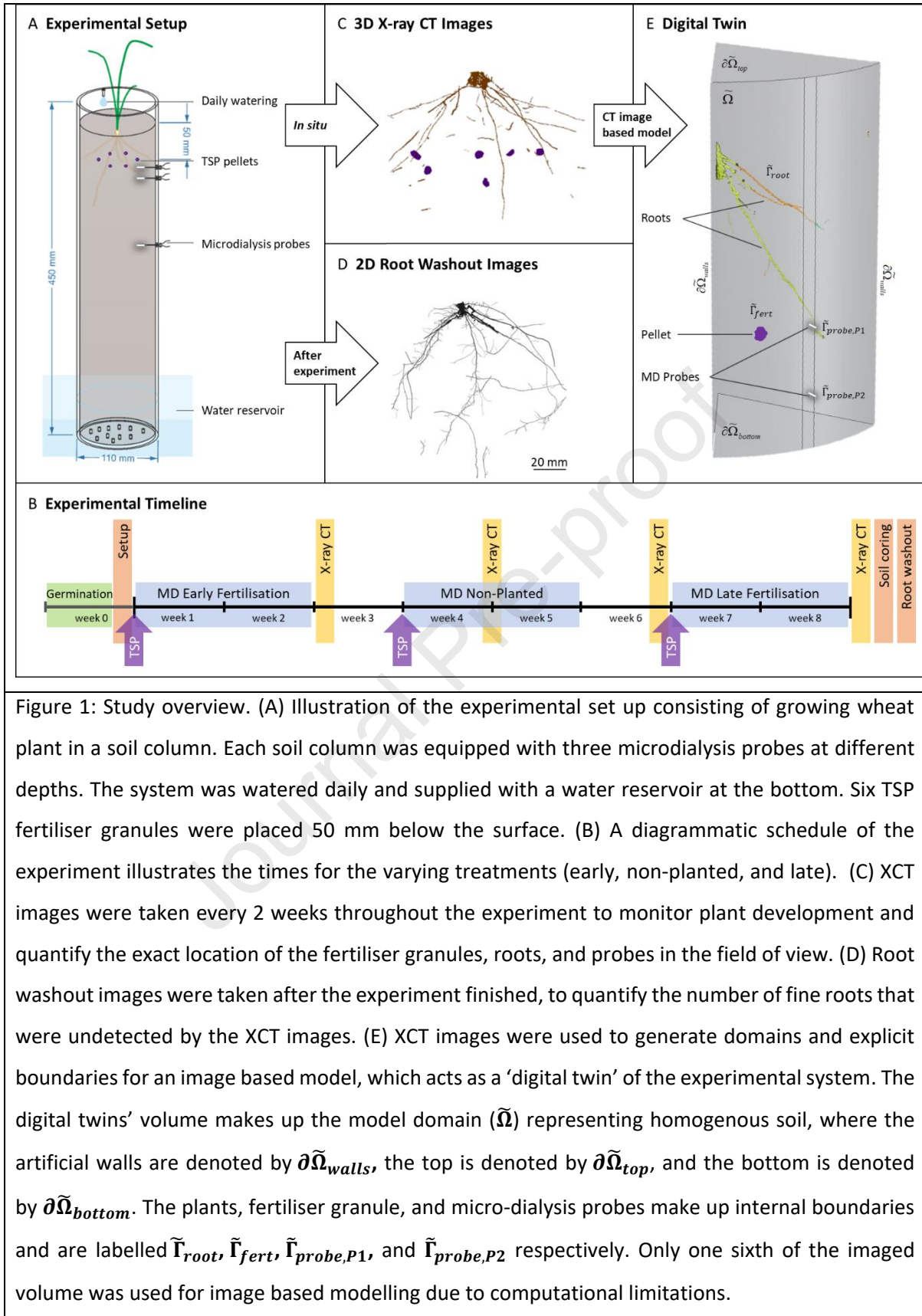
147 The experimental setup was adapted from previous studies (Ahmed et al., 2016; Williams et al., 2022)
148 that integrated microdialysis sampling into an assay suitable for X-ray Computed Tomography (CT).
149 PVC tubes with an external diameter of 110 mm and a height of 450 mm were used as support for the
150 soil columns. Sandy clay loam Eutric Cambisol soil from an agricultural grassland in the Henfaes
151 Research Station in Abergwyngregyn, Wales (UK; 53°14'N, 4°01'W) was oven-dried at 70°C overnight
152 and sieved to pass 2 mm. Dry bulk density was $\rho_b = 1.26 \pm 0.01 \text{ g mL}^{-1}$. The soil properties are reported
153 in Supplementary Table S1. Olsen-P test results for this soil have been extensively reported in previous
154 publications (Oburger et al., 2009; Oburger et al., 2011; Ahmed et al., 2016) and the soil has been
155 contained on site in sealed bags ever since. The measured Olsen-P concentration is 12.6 mg L^{-1} , which
156 is classified as category 1 in the Department of Environment, Food and Rural Affairs (DEFRA) UK system
157 (i.e. some response to P fertiliser expected) and has a recommendation of $40 \text{ kg of P ha}^{-1}$ of fertilisation
158 to achieve optimal yields (AHDB, 2023). In this work, we will refer to low-STP soil as soil of category 1
159 and below, as such, our soil will be classified as a low-STP soil. Soil moisture content was initially
160 adjusted to 12.5% and approximately the same mass of wet soil was added to each column (3469 ± 5
161 g). The columns were then transferred into a growth cabinet with a 16/8 h day/night cycle, 20°C air
162 temperature and 50% relative humidity. An automatic watering system was setup to deliver 90 mL of
163 deionized water per day (DI; resistivity = $12 \text{ M}\Omega$) to each pot and a tray with DI water to a height of
164 about 5 cm placed underneath the columns complementing the irrigation via capillary action. Soil
165 nutrients were added weekly as 25 mL of custom made full strength P-free Hoagland's solution
166 (Hoagland and Arnon, 1950) per pot and additional N and K were supplied once after shoot emergence
167 as NH_4NO_3 at a rate of $62 \text{ kg (N) ha}^{-1}$ and KCl at a rate of $50 \text{ kg (K) ha}^{-1}$, respectively. Phosphorus was
168 supplied as triple super phosphate (TSP) granules at $80 \text{ kg (P}_2\text{O}_5) \text{ ha}^{-1}$, by adding six granules per tube
169 (average mass of the single granule $35 \pm 2 \text{ mg}$) at 5 cm depth, 2.5 cm from the pipe walls to avoid
170 preferential water flow patterns, and equidistant from each other (Figure 1A). Spring wheat seeds
171 were germinated on damp paper for a week and then transferred into soil sowing three seeds per pot.
172 After one week from sowing, pots were thinned and only the most vigorous seedling was kept in each
173 pot.

174 Three pots were set up for each of the following treatments: an "early fertilisation" treatment where
175 TSP granules were added 1 week after planting, a "late fertilisation" treatment where TSP granules

176 were added 6 weeks after planting (when the roots are expected to have already reached the depth
177 of the granules (Ahmed et al., 2016)), a “non planted” treatment where TSP granules were applied,
178 but no plant was included, and a “blank” treatment where a plant was grown, but no fertiliser was
179 added. A total of 12 pots were setup.

180 The overview of the experimental setup and design is outlined in Figure 1A while a timeline of the
181 experiment is shown in Figure 1B. Wheat plants were sowed into each “early fertilisation”, “late
182 fertilisation” and “blank” treatments with replicates; total of 9 plant samples. Six TSP fertiliser granules
183 were added to each “early fertilisation”, “non planted” and “late fertilisation” treatments, respectively
184 at week 1, week 4 and week 7 after sowing (Figure 1B). Microdialysis sampling was carried out for 14
185 days from fertiliser application for a total of 460 dialysate samples. One blank treatment replicate was
186 monitored during all three of the measurement periods with one microdialysis probe placed at 2.5 cm
187 below the depth at which the granules were placed in the fertilised columns (about 50 samples in
188 total). Root imaging was carried out every two weeks by XCT (Figure 1C), while root washout and 2D
189 imaging was performed at the end of week 8 for all plant samples (Figure 1D). Before disrupting the
190 soil columns to wash out the root system, a smaller 1.5 cm diameter soil core was extracted and
191 sectioned for subsequent total P quantification at various depths.

192



194 2.2 Soil solution microdialysis sampling and analysis

195 Three CMA 11 metal-free microdialysis probes (4 mm; 6 kDa cut-off; CMA Microdialysis AB, Sweden)
196 were inserted in each tube at 1.0, 2.5 and 11.5 cm depth from the TSP granule layer, respectively for
197 the “early”, “late” and “non planted” pots. For blank treatments, one single probe was added to each
198 pot at a depth of 2.5 cm from the virtual granule level, as P diffusion dynamic is not expected in low-
199 STP soil in the absence of a local P source (Petroselli et al., 2021). Indeed, we observed that the P
200 concentrations in the soil solution detected by the probes in the blank treatment during the three
201 subsequent sets of sampling do not show any particular trend associated with P release into or
202 removal from the soil solution during the whole 8 weeks period, with an average value of 0.1 ± 0.05
203 ppm (Supplementary Material Figure S1). These results show that sorbed P into soil solids as well as
204 microbial activity and water flow due to watering from the top of the soil column are negligible in the
205 undisturbed experimental system.

206 The probes were aligned below one of the granules in order to maximize detection. Probes were
207 perfused with MilliQ water (18 M Ω) at a rate of $3.3 \mu\text{l min}^{-1}$ (McKay Fletcher et al., 2019; Petroselli et
208 al., 2021) using a PHD 2000 Programmable Syringe Pump (Harvard Apparatus, UK). Sampling time was
209 set to 2 h for the first four samples and 12 h for the rest of the experiment. The obtained dialysate
210 samples were stored in the fridge at +4°C until analysis in airtight containers. Prior to quantification,
211 dialysate samples were spiked with internal standard elements (Be, In and Re) in a 3% HNO₃ solution
212 to account for matrix drift correction. Quantitative elemental analysis was performed by means of
213 Inductively Coupled Plasma Mass Spectrometry (ICP-MS) at the University of Southampton National
214 Oceanography Centre. A single quadrupole XSeries2 (Thermo-Scientific) was used and seven custom
215 calibration standards were prepared from single element certified standards (Inorganic Ventures TM).

216 Raw microdialysis data reflects diffusion rate into the probe not soil solution concentration directly.
217 Therefore, dialysate concentrations were converted into soil solution concentrations using a
218 correction factor measured in a previous study (Petroselli et al., 2021) which compared a direct
219 (suction cup) sampling method with microdialysis sampling for the same soil solution concentrations.

220 Due to the characteristics of the sampling and analysis methods, all presented data of P in dialysates
221 refer to elemental P quantification in samples obtained by passive diffusion of small solute molecules
222 from the soil solution into the dialysis solution. The sampled P compound speciation is beyond the
223 scope of the present paper, however, due to the probe physical features (6 kDa cut-off), we can
224 exclude the sampling of larger molecules (such as DNA), microbes and hydrophobic molecules. We
225 will therefore be referring to P concentrations including the contributions from all the P compounds
226 that are compatible with our sampling technique.

227 2.3 Soil sampling and analysis

228 Total P concentration in soil was determined at the end of the experiment by means of total acid
229 digestion followed by ICP-MS analysis. Soil was sampled with a 1.5 cm diameter soil corer and the
230 samples were subjected to total acid digestions with a custom HF/HClO₄ protocol until total digestion
231 was achieved. The digestion protocol details can be found in the Supplementary Material section
232 1.1.2. Quantified elements and calibration are analogues to the ones used for the dialysate samples.
233 These results are not further discussed in the paper because they don't show any noteworthy trend
234 or differences between the treatments. However, averaged data are shown in the Supplementary
235 Material Figure S11.

236 2.4 X-ray Computed Tomography

237 X-ray computed tomography scans were carried out to visualise the growing roots at 2, 4, 6, and 8
238 weeks after planting (Figure 1 B and C). The scans detected the precise location of the microdialysis
239 probes and TSP granules in the system and time-resolved location of the growing plant roots. Before
240 scanning, watering was ceased for at least 1 day to enhance contrast.

241 Scans were carried out using a custom 450/255 kVp Hutch XCT scanner at the μ -VIS X-ray Imaging
242 Centre, University of Southampton, UK. Each scan used 3142 projections, with eight frames per
243 projection and a 134-ms exposure per frame. The energy chosen was 150 kV at 210 μ A. The resulting
244 voxel size was 60 μ m. These parameters were chosen to provide sufficient contrast to visualize the
245 roots, soil, probes, and fertilizer granule while minimizing the scan time (each scan took approximately
246 60 min). The voxel size was the smallest possible so that the entire column diameter fitted within the
247 field of view, to give the highest resolution possible. Scans were reconstructed with a filtered back-
248 projection algorithm in CTPro (Nikon Metrology).

249 **2.4.1 Image processing**

250 Roots were segmented from the surrounding soil using a custom workflow, implemented in a
251 combination of the FIJI distribution of ImageJ (Schindelin et al., 2012; Rueden et al., 2017), a free,
252 open-source software package for image processing and analysis, and Dragonfly (ORS, Quebec,
253 Canada), a commercial piece of image processing, analysis, and visualisation software. Segmented
254 root systems were aligned to label roots that emerged at each time point (Figure S1) The full workflow
255 is described in the Supplementary Material.

256 Due to imaging constraints, any roots smaller than 60 μ m were not visible in the image since this is
257 the size of one voxel, while segmentation will also remove further small roots, at a minimum those
258 below 120 μ m in diameter due to a 1 pixel opening step included in the workflow. This means that

259 only primary roots could be segmented. Segmented root systems were spatially registered across time
260 points to allow the emergence time of each part of the root system to be identified (see
261 Supplementary Material for full details). The granules and microdialysis probe membrane regions
262 were also added to the segmentations based on the XCT images.

263 For blank treatments where no fertiliser granules were present, a mock granule was added digitally in
264 the images to generate comparative measurements. The mean granule diameter was chosen by
265 randomly selecting a replicate (L3) and measuring the mean granule diameter of all six granules in the
266 image then calculating a mean of means, giving a diameter of 3.8 mm. A sphere with diameter 3.8 mm
267 was drawn onto the image using the 3D segmentation tools in Dragonfly. All were placed with their
268 centroids on a single plane to match as closely as possible the real granules in the fertilised treatments.

269 **2.4.2 Image measurements**

270 To measure the minimum distance between each probe and the nearest P granule, an exact Euclidean
271 distance transform was generated from the granule image. Then, the grey value at the coordinates of
272 the tip of each probe was measured to give the minimum distance to a granule.

273 **2.4.3 XCT root measurements**

274 Segmented root systems were measured using the BoneJ plugin of ImageJ (Doube et al., 2010). Each
275 root system was skeletonised (thinned to a single line of pixels). The root length was then measured
276 by counting the number of white (root skeleton) pixels and converting into mm.

277 **2.4.4 Root washout root measurements**

278 At the end of the experiment, and after soil coring, the roots were washed out of the soil and
279 photographed to investigate the proportion of roots captured by the XCT imaging. Additional samples
280 were also used for this so that $n=4$ for all treatments. Roots were removed from the soil by hand,
281 washed gently with running water to remove as much bound soil as possible then rinsed using
282 deionized water (12 M Ω). Roots were then submerged in water to allow roots to spread out and
283 photographed from below using a Panasonic DMC-FZ330 camera (resolution 4000x3000 pixels) with
284 approximately 1 pixel = 60 μ m. Images were cleaned using a custom image processing workflow in
285 ImageJ as detailed in the Supplementary Material.

286 Skeletons were generated for each root system using Skeletonise 2D/3D in ImageJ. Additionally, the
287 'Local Thickness' function in ImageJ was applied to the binary root washout image to determine the
288 radius of each root pixel. Since the XCT imaging approach did not have the resolution to segment and

289 measure the smaller roots, we instead used the root washout light microscopy images to determine
290 experimental root length and root surface area.

291 The local thickness and skeleton image of the binary root washout image were used to measure root
292 length and surface area. To calculate the total root length of each replicate, we counted the length
293 contribution of each pixel in the skeletonised images. Length between pixels in contact (including
294 diagonals) was calculated *via* Euclidian distance of their central points. To calculate the root surface
295 area we assumed that each pixel of root in the skeleton image was a perfect cylinder with a diameter
296 value associated with the local thickness map. Each pixel in the skeleton then has an associated surface
297 area. The total root surface area was then the sum of all pixel root surface area contributions. Total
298 root length and root surface area was calculated using Python 3.8 (VanRossum and Drake, 2010) after
299 exporting the skeleton and local thickness images from Fiji.

300 2.5 Plant biomass measurements

301 Above ground biomass was recorded fresh and after air-drying, while for below ground biomass, the
302 fresh mass could not be determined due to the washing procedure and it was thus weighed after air-
303 drying only. Plant material was freeze-dried, ground and digested prior to ICP-MS analysis. The
304 digestion protocol used in this case involved the use of a MARS6 microwave digestion system (CEM
305 corporation, USA) and a H₂O₂/HNO₃ reagent mixture (details in the SM section 1.1.3). The obtained
306 samples were then analysed by ICP-MS after an appropriate dilution.

307 3. Theory and Calculation

308 3.1 Digital Twin

309 3.1.1 Summary and aims

310 An image-based model of P transport in soil was linked to the geometry derived from the XCT scans
311 producing a digital twin of each experimental replicate. The following experimental details were
312 accounted for in the model development: root geometry as measured from XCT scans with roots
313 growing over time to match experimental data, microdialysis sampling time and position, timing and
314 position of fertiliser application. The lowest probe was not visible in the XCT data but was used as a
315 lower boundary condition. Importantly, full mass balance was achieved accounting for both P
316 removed by soil and by the probes. We excluded P coupling to moisture dynamics (no P-advection
317 (Tinker and Nye, 2000)) because of constant moisture conditions ensured by regular watering, and we
318 also neglect the effects of root organic-acid exudation (Demand et al., 2017; McKay Fletcher et al.,
319 2019; McKay Fletcher et al., 2020). Further details of the model construction are available in the
320 Supplementary Material.

321 The modelling of P removal from the soil solution required choosing appropriate P-soil interactions
 322 (Ruiz et al., 2021). Our experiment does not allow us to disentangle the P removing processes (i.e.
 323 sorption, precipitation and microbial activity), therefore we focused on the overall effect of P removal
 324 from the soil solution. We compared two different soil P binding models, namely a standard an
 325 equilibrium (Buffer Power, (Barber, 1995)) and a dynamic (Absorption-Diffusion) description of the P-
 326 soil retention. We compared the model results to the experimental microdialysis results to determine
 327 which was more suitable for modelling P transport/retention at these spatial and temporal scales.

328 3.1.2 Model description

329 We generated an image-based model as a digital twin to aid in our understanding of the physical
 330 phenomena evident in the experimental results. We used the XCT scanned geometry of each replicate
 331 to generate a finite element mesh used as domains to solve the P models. Due to the high
 332 computational cost to run simulations on such detailed domains, it was only possible to simulate a 6th
 333 of the domain (i.e. $\tilde{\Omega}$ represents a sixth sector of the full experiment, Figure 1E), with each sector
 334 centred about the location of a micro-dialysis probe in each. $\tilde{\Omega}$ represents three-dimensional
 335 homogenous soil with volumetric water content $\tilde{\phi}_l$ [m³ of liquid m⁻³ of bulk soil] and volumetric soil
 336 solid content $\tilde{\phi}_s$ [m³_{solid} m⁻³_{bulk}]. We first present the full model with first-order kinetics describing P-
 337 soil reactions then describe the assumptions required to derive both the Buffer Power (equilibrium)
 338 model and the Absorption-Diffusion (dynamic) model.

339 To quantify the phosphorus dynamics in the microdialysis experiments, we start by describing the
 340 transport dynamics of dissolved phosphorus (P) in a bulk soil domain. Let \tilde{c}_l [mol m⁻³_{liquid}] represent
 341 the concentration of phosphorus compounds in soil solution and \tilde{c}_s [mol m⁻³_{solid}] represent the
 342 concentration of phosphorus compounds retained by the soil (i.e. removed from the soil solution). We
 343 assume P only moves by diffusion in soil pore water and the P-soil reaction is governed by first order
 344 kinetics:

	$\phi_l \frac{\partial \tilde{c}_l}{\partial \tilde{t}} = \tilde{\nabla} \cdot (\phi_l \tilde{D} f \tilde{\nabla} \tilde{c}_l) - \phi_l \tilde{\beta}_1 \tilde{c}_l + \phi_s \tilde{\beta}_2 \tilde{c}_s, \quad \tilde{\mathbf{x}} \in \tilde{\Omega}, \tilde{t} \geq 0,$	1
--	---	---

345 where \tilde{D} [m²_{liquid} s⁻¹] is the diffusivity of solution P in free liquid, f [-] is the geometric pore-space
 346 impedance to diffusion, $\tilde{\beta}_1$ [s⁻¹] is the effective absorption rate and $\tilde{\beta}_2$ [s⁻¹] is the desorption rate. We
 347 again stress that the effective absorption rate is a general sink term that accounts for sorption,
 348 precipitation and microbial activity. We note that P reaches the microdialysis probes on diffusive time
 349 scales (demonstrated in results section), thus it suffices to neglect advection even in the presence of
 350 daily watering from the top of the soil column. \tilde{c}_s is assumed to be immobile and is tracked by
 351 conservation of mass (see Supplementary Material for details). At the imaged root interface ($\tilde{\Gamma}_{root}(t)$)

352 the boundary evolves over time in accordance to the XCT imaged roots, and the uptake is modelled
 353 based on Michaelis-Menten kinetics (Barber, 1995).

354 The microdialysis probes sample P *via* diffusion, thus they are included in the simulations as surface
 355 boundary sinks ($\tilde{\Gamma}_{probe,i}(\tilde{t})$). Since only the two probes closest to the soil surface were imaged using
 356 XCT we only include these probes in the model (Figure 1E). The times that the probe boundaries
 357 $\tilde{\Gamma}_{probe,i}(\tilde{t})$ are active are in direct accordance with the experimental sampling protocol.

358 The fertiliser granule is assumed to release a fixed quantity of P at an exponentially decreasing rate.
 359 The fertiliser boundary $\tilde{\Gamma}_{fert}(t)$ is activated at the time of granule deployment, which is different for
 360 early and late treatments. No flux conditions are assumed at the top of the domain ($\partial\tilde{\Omega}_{top}$), where P
 361 is not expected to leave, and at the artificial walls ($\partial\tilde{\Omega}_{walls}$), given our assumption that any adjacent
 362 sectors would be identical in concentration (each would contain a P pellet in the same position). See
 363 the Supplementary Materials for all details of the different boundary and initial conditions.

364 3.1.3 Modelling buffer power and Absorption-Diffusion

365 Both the Buffer Power (BP) and the Absorption-Diffusion (AD) models can be derived from eq 1
 366 considering two different scaling arguments. The first argument (*i.e.* the Buffer Power argument)
 367 assumes that the rates of absorption and dissolution are similar in magnitude (*i.e.*, $\bar{\beta}_1 \sim \bar{\beta}_2$; Barber,
 368 1995) and the reaction rates are much larger than the characteristic timescale so that we can assume
 369 the P-soil reactions are instantaneous relative to the diffusion time-scale (see Supplementary Material
 370 for more details). This set of assumption leads to the Buffer Power (BP) model (Ruiz et al., 2021):

Buffer Power (BP) model	$(b + \phi_l) \frac{\partial c_l}{\partial t} = \nabla \cdot (\phi_l D_f \nabla c_l), \quad \mathbf{x} \in \Omega.$	2
----------------------------	---	---

371 where $b = \frac{\phi_l \bar{\beta}_1}{\bar{\beta}_2}$. While the Buffer Power model is suitable to describe transport of P in larger scale soil
 372 systems, preliminary results suggested it may not be able to capture all the features of the
 373 experimental within season shorter time and length scale results (see Results section). Therefore, we
 374 seek an alternate model that can better capture microdialysis results. As motivation for the alternate
 375 approach, we note that the assumption $\bar{\beta}_1 \sim \bar{\beta}_2$ in the buffer power derivation is not valid for soils with
 376 high sorption capacity like that used in this experiment. Soils with high sorption capacity are
 377 characterised by high buffer powers, ranging from 40-1000 and typically in the hundreds (Barber,
 378 1995). Since $b = \frac{\phi_l \bar{\beta}_1}{\bar{\beta}_2}$ and ϕ_l will be on the order of 0.1-0.6 and b on the order of 40-1000, it follows
 379 that $\bar{\beta}_1 \gg \bar{\beta}_2$. We use this to define the Absorption-Diffusion reduction. For this model, we neglect
 380 the smallest terms (*i.e.* $\bar{\beta}_2$). As such, eq 1 reduces to:

Adsorption-Diffusion (AD) model	$\phi_l \frac{\partial c_l}{\partial t_1} = (\nabla \cdot (\phi_l D f \nabla c_l)) - \phi_l \beta_1 c_l, \quad \mathbf{x} \in \Omega$	3
------------------------------------	---	---

381 In this study, we compare results from the Buffer Power model (BP, eq. 2) and the Absorption-
 382 Diffusion model (AD, eq. 3) to determine which is most appropriate for modelling our within season
 383 experimental system. All the details about the model derivations and the selection of parameters are
 384 included in the Supplementary Material in the Modelling methods section.

385 3.1.4 Data fitting

386 **Fitting the Absorption-Diffusion model to the microdialysis experiment**

387 The experimental microdialysis probes passively take up P from the soil solution *via* diffusion across a
 388 membrane. This results in a concentration of P in the dialysate due to the flux of P across the probe
 389 membrane over the sampling timescale. However, flux of P is influenced by how closely the probe
 390 contacts the soil, the local saturation of the soil and other factors which affect the measurement in
 391 addition to soil solution concentration. Thus, a set of parameters were determined for each probe to
 392 account for the variability in probe diffusion rates, probe soil-water contact and natural soil variability.
 393 Each fitting parameter controls particular aspects of the model probe measurement, see Figure 2A.
 394 The geometric impedance factor f controls the speed of diffusion of P from the fertiliser granule
 395 towards the probes. This remained fixed across the samples. The absorption rate $\tilde{\beta}_1$ controls how
 396 much P was bound to the soil (i.e. removed from the soil solution; Figure 2A) and was allowed to vary
 397 between tests, although this was in fact consistent for all tests except one. For all of the tests, we fit
 398 different values of probe uptake rates $\tilde{\delta}_i$ for each replicate for the two imaged probes in the event
 399 that probes further from the granule had a higher uptake. The parameters that minimised the square
 400 sum (over probe and sample time) difference between the model probe uptake and the experimental
 401 measurement was deemed the best fit parameters for each replicate, see Supplementary Materials
 402 for exact details on the objective function.

403 3.1.5 Numerical Experiments

404 **Comparing the Buffer Power model and Absorption-Diffusion model to the experimental** 405 **measurements**

406 The suitability of the two models (*i.e.* Absorption-Diffusion and Buffer Power) for describing the
 407 experimental system was assessed based on two comparisons. The first comparison was between the
 408 probe uptake estimated by the model for each microdialysis probe and the uptake measured by that
 409 probe in the experiment. Unlike the Absorption-Diffusion model, preliminary simulations suggested
 410 that the Buffer Power model could not characteristically match the experimental probe
 411 measurements as the theoretically observed uptake curve morphology was radically different from

412 experimental observations (i.e. Buffer Power model was only able to characterise the rise in
413 concentration but not the fall), thus we did not perform a rigorous data fitting routine for the Buffer
414 Power model. To illustrate this, we show the model probe uptake for the Buffer Power model using
415 two extreme values for buffer power, $b = 1$ and $b = 40$ to demonstrate that no matter what value
416 for $b, f, \tilde{\delta}_{P1}$ or $\tilde{\delta}_{P2}$ is chosen, the buffer model will not be able to match the experiential microdialysis
417 probe uptake measurements. Figure 2 illustrates the characteristic differences between the
418 Absorption-Diffusion model and Buffer Power model, and it highlights the effect each parameter has
419 on the modelled microdialysis probe measurement. The Absorption-Diffusion model can generate a
420 pulse of P measured by the microdialysis probe (Figure 2A). Increasing the geometric impedance
421 parameter f in the Absorption-Diffusion model, increases the time it takes for the P from the fertiliser
422 granule to reach the probe (Figure 2A). The absorption rate $\tilde{\beta}_1$ controls the width (time the pulse lasts
423 for) and the measured concentration of the pulse. Additionally, the absorption rate determines the
424 decay rate of the pulse of P from the fertiliser in the soil solution. The probe uptake rate $\tilde{\delta}_i$ controls
425 how much P is taken up by the probe and thus the intensity of the peak. However, the probe uptake
426 will saturate when the probe has depleted all locally available P.

427 Many of the parameters interact similarly in the Buffer Power model as they do in the Absorption-
428 Diffusion model. The geometric impedance factor f controls the speed at which P from the granule
429 reaches the microdialysis probe and $\tilde{\delta}_i$ controls how much P is taken up by the probe with a maximum
430 amount dependent on locally available P (Figure 2B). Similar to f , the buffer power b limits the speed
431 of diffusion to the probe, (Figure 2B). For both models there is interplay between the parameters, for
432 example if f increases there is more time for P to be removed from the soil solution, and thus the
433 peak in model microdialysis measurement would be later in time and lower in magnitude. Additionally,
434 the distance of the probe to the fertiliser granule will also affect the model probe measurements.

435

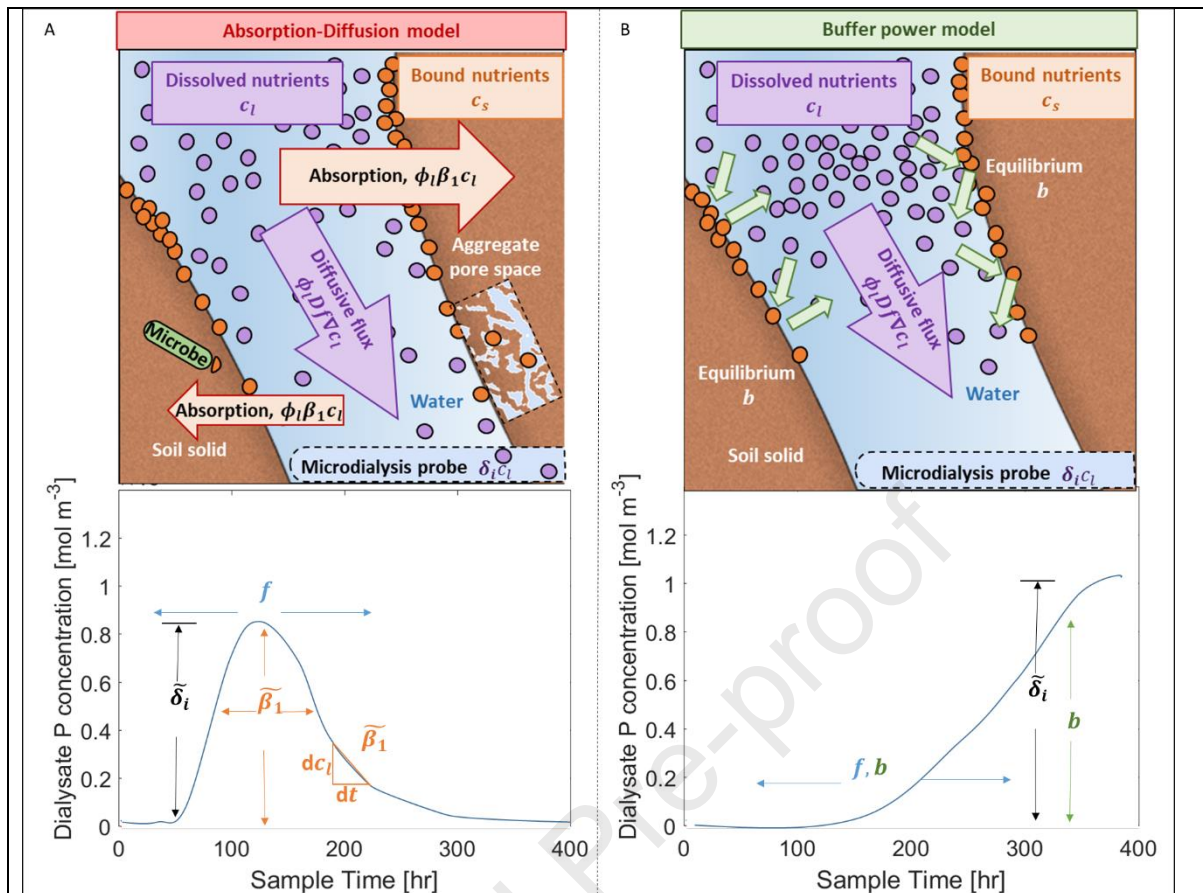


Figure 2: Visual description of the effect of the parameters on model probe measurement for (A) the Absorption-Diffusion model and (B) the Buffer Power model. (A) The Absorption-Diffusion model considers removal of solute from the soil solution to be the dominating reactive process (e.g. surface binding, aggregate trapped, microbial activity). As such, dialysis probes are expected to sample concentrations of P as they gradually diminish from the solution space based on the absorption rate $\tilde{\beta}_1$. (B) The Buffer Power model considers that the absorbed and desorbed P are in a constant state of equilibrium based on the ratio between absorption and desorption rates (*i.e.* the buffer power b). The buffer power acts to impede rates of transport, thus the probes are expected to sample P at a delayed rate.

436

437 For the second comparison, each model's root P uptake was compared to the plant total P
 438 determination to establish how well they estimated P uptake. The equation for calculating root P
 439 uptake in the model can be found in the Supplementary Materials. For the Absorption-Diffusion
 440 model, the set of parameters that best fit the microdialysis probe measurements for each replicate
 441 were used in this numerical experiment. For the Buffer Power model, we used the Absorption-
 442 Diffusion fit uptake parameters and selected $b = 40$ based on previous microdialysis experiments
 443 (McKay Fletcher et al., 2019) or as 1 to simulate a low buffering soil. We also compare the model P

444 uptake efficiency of both models to the experimental measurement of P uptake efficiency. In this
445 paper, P uptake efficiency is defined as total plant P uptake per total root surface area and captures
446 how much P the plant takes up per carbon investment in the form of root surface area. Since the XCT
447 imaging did not have the resolution to capture the smallest roots, the root surface area in the models
448 is an underestimate. However, it is likely the roots that were included in the model are in close
449 proximity to those that were missed by the XCT imaging and we expect that the roots in the model
450 are representative of all roots in the experiment's geometric arrangement. Thus, we expect the model
451 will underestimate total P uptake, but be able to capture qualitative differences between treatments.
452 Additionally, we expect the modelled P uptake efficiency to be more in line with the experimental
453 calculation quantitatively because the XCT measured roots were likely to be representative of the
454 location of all roots.

455 4. Results

456 4.1 Root measurements

457 First, we compared the root traits between replicates and treatments to test whether the treatments
458 had resulted in any root responses or differences in plant growth. The mean fresh shoot mass for the
459 Non-fertilised treatment was slightly greater than the Early ($p < 0.05$), but not significantly different
460 from the Late treatment, and there was no difference between the Early and Late treatments (see SM
461 Figure S2). The root mass did not differ significantly between the treatments, however, based on
462 washout images (Figure S3), the mean total root length was significantly higher for the Late treatments
463 compared with the Early treatment and the Blank treatment ($p < 0.05$ and < 0.05 respectively) (Figure
464 S3). Based on the root length measured from the XCT data (Figure S4), there was no significant
465 difference in mean total root length between the fertilised treatments at 8 weeks (the equivalent time
466 point to the washout experiments), although the mean total root length was consistently the highest
467 through the 8 weeks in the Late treatment. Looking at the XCT data, the difference in total root length
468 occurred from 2 weeks of growth and persisted throughout the subsequent period (Figure S4).
469 Although the XCT data underestimates the total root length as the finest roots are not captured, nor
470 are roots that grow beyond the depth of the XCT scan, there is a correlation ($r^2 = 0.458$) between the
471 total lengths measured from the XCT and from the washed-out roots (Figure S4).

472 We found no significant differences between any treatments in number of lateral roots with depth or
473 mean lateral root density (Figure S5), or root length density with depth (Figure S6). Although we
474 predicted there might be a proliferation of roots near the fertiliser granule when it was added at 8
475 weeks in the Late treatment, this was not observed in the XCT (Figure S7). In all but one case, the
476 mean root-soil distance decreased as the roots explored more of the soil through the weeks (Figure

477 S8), but the roots did not explore the soil to differing extents with respect to the fertiliser treatment
478 (as measured by the mean root-soil distance measure) (Figure S8).

479 4.2 Microdialysis

480 Microdialysis sampling was carried out for all replicates of Early Fertilisation, Late Fertilisation and
481 Non-planted treatments for the two weeks following fertiliser application (Figure S10). Averaged
482 elemental P concentrations in the soil solution were determined by microdialysis sampling for each
483 treatment, and are reported in the Supplementary Material Figure S10 (first row); P concentrations
484 for each individual replicate of Early and Late fertilisation treatments are shown in Figure 3 (dots and
485 dashed lines). The common trend detected by most of the probes is consistent with what was
486 expected based on Petroselli et al. (2021). The probes detect a phosphorus concentration pulse in the
487 soil solution, characterised by a rapid rise in P concentrations between 0 to 80 hours after fertiliser
488 application, a maximum that was reached between 50 to 160 hours after fertilisation and a
489 subsequent decrease to approximately pre-fertiliser concentrations after 6-7 days.

490 Missing data in Figure 3 can be attributed to low P concentrations that are below the limit of detection
491 and, in some cases, to probe failure. The latter is not unusual when these fragile devices are used in
492 soil, however, the setup design allowed for access and replacement of the probes during the
493 experiment, limiting this issue to very few sampling points. The difficulty in determining low P
494 concentrations, on the other hand, depends on various factors concerning the use of micro-sampling
495 probes such as (1) the dilution operated by the MD probes on the sample (Petroselli et al., 2021), (2)
496 the small size of the probe compared to the size of the pot that implies that the measurements are
497 representative of a very local environment, (3) detectable concentrations depend very strongly on
498 granules-probe vertical alignment which is also linked to the length of the probe that determines how
499 far the probe can penetrate into the soil considering that it needs to be accessible from the outside of
500 the tube. These issues may be linked to the probe positioning and alignment which, together with the
501 limited control on the probe's incline at insertion, resulted in a high variability in the data collected
502 from different replicates.

503 In light of these considerations, the replicates are discussed individually and the exact location of the
504 MD probes' membranes (position and angle) was determined from the XCT scans in order to support
505 the interpretation of the MD results. The obtained pellet-probe distances are reported in Table 2.
506 Intuitively, the highest P concentrations were recorded for the L1 replicate, where the distances
507 between the probes and the granule are the shortest.

508 *Table 1: Summary of distances of each microdialysis probe to its nearest fertiliser granule. Each value is calculated from the*
509 *XCT scan and is in mm. z-distance is the distance to the fertiliser granule along axis in the direction of the column height, a*

510 *negative z-distance means the probe is above the fertiliser granule. xy-distance is the distance to the fertiliser granule in the*
 511 *plane perpendicular to the height axis. Distance is the 3D Euclidean distance to the fertiliser granule.*

	E1		E2		E3		L1		L2		L3	
	P1	P2	P1	P2	P1	P2	P1	P2	P1	P2	P1	P2
z-distance	3.0	18.1	4.1	19.4	7.8	21.9	0.9	14.2	9.9	27.0	-4.9	13.0
xy-distance	14.1	14.7	12.7	12.1	11.8	8.9	7.52	8.8	18.6	18.5	13.6	13.8
Distance	14.4	23.3	13.3	22.9	14.1	23.6	7.58	16.7	21.1	32.7	14.5	18.0

512

513 The probes' nominal distances from the vertically aligned granule are P1 = 1.0 cm, P2 = 2.5 cm and P3
 514 = 11.5 cm, however, probe's incline and soil compaction after setup can significantly modify the
 515 relative distances between the granule and the probes. This has been observed in a few cases where
 516 the second probe (P2) detects the P concentration pulse at the same time as the first probe (P1), see
 517 Figure 3 C and D that correspond to E2 and L2. In these two cases, the vertical distance between the
 518 two probes is less than 2 cm which is compatible with the span of the pulse observed in the same soil
 519 (Petroselli et al., 2021). Additionally, in L1, L2, and L3 (Figure 3 B, D and F) the maximum concentration
 520 recorded by probe P2 is higher than probe P1. In the L3 case, the first probe ended up above the
 521 granule (vertical distance -4.9 mm), explaining the very low concentrations and the diffusive trend, in
 522 line with what was observed in Petroselli et al. (2021). In the L1 and L2 cases, this effect cannot be
 523 attributed to the probe-granule distance as the probes show a correct vertical distancing and a
 524 consistent horizontal alignment (Table 2).

525 The E1 and E3 replicates show P concentrations that are one order of magnitude lower than the other
 526 replicates (10^{-4} versus 10^{-3} mol m⁻³). The missing data points and the high variability in the data are
 527 explained by the low concentrations, which often fall below the limit of detection or within the
 528 experimental noise range. As the distance of the probes from the granule in these two cases is not
 529 dissimilar to the other replicates both vertically and horizontally, we exclude this to be responsible for
 530 the low observed concentrations. The anomaly could be therefore attributed to more local effects,
 531 such as the presence of air bubbles near the MD membrane that impede the diffusion of solutes
 532 towards the probe, the membrane drying which could lead to membrane damage and rupture,
 533 observed in the E1 case, or soil heterogeneity. The obvious way to increase the concentration of P in
 534 the MD samples is to use a membrane with large surface area/length. However, this would have at
 535 least two challenges: (1) longer membrane would be more fragile and hence more easily breakable in
 536 the soil and (2) larger membrane would result in larger soil disturbance hence in more other
 537 measurement artefacts.

538 4.3 Modelling results

539 For the most part, we found that our modified Absorption-Diffusion model was better able to capture
540 the P dynamics in the soil solution than the standard Buffer Power model. Therefore, in this results
541 section we start by comparing the Absorption-Diffusion model to the experimental data before
542 moving onto comparing the two models. Figure 3 shows the results of the Absorption-Diffusion model
543 (solid lines) alongside the experimental results. The model predicts that all probes, apart from P1 in
544 E1, should detect a phosphorus pulse. Moreover, the model predicts that the pulse will always reach
545 the closer probe (P1) before being detected by the second one (P2) even though the experimental
546 data show that in some cases the pulses are detected simultaneously by the two probes (Figure 3 C
547 and D). Regarding the relative concentrations detected by the two probes, the model correctly
548 captures the main variations due to the probe positioning (e.g. L3, Figure 3F), however, when the
549 probes are close enough to detect the pulse at the same time (e.g. L2, Figure 3D), the observed
550 differences in the absolute concentration values lose significance as they might be affected by the
551 pulse timing effect that cannot be captured because it is below the experimental time resolution.

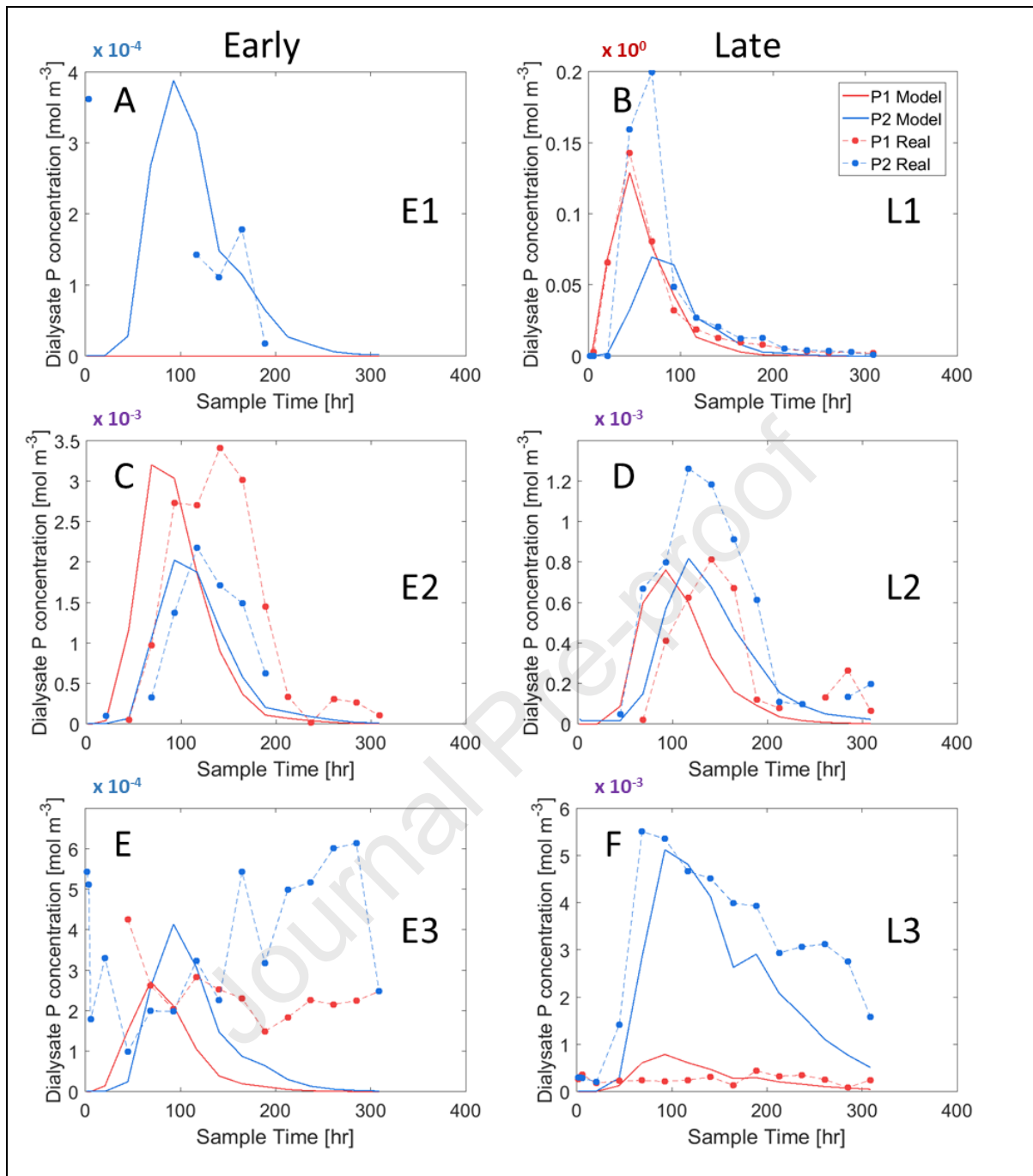


Figure 3: Phosphorus concentration in the soil solution is reported in function of sample time. Microdialysis experimental results (dots + dashed lines) and Absorption-Diffusion digital twins (solid lines) for Early fertilisation (E1, E2, E3) and Late fertilisation (L1, L2, L3) treatments replicates. Red lines refer to the probe closest to the granule (P1) while blue lines represent the middle probe (P2). Refer to Table 2 for probes-granule distances and to Table 3 for the associated model parameters. Please note that the panels show different scales on the y-axis (blue 10^{-4} , purple 10^{-3} , and red 10^0), linked to the variability of the data. This allowed us to clearly show the trends and the accordance of the experimental data with the model.

552 The fitted parameters for the Absorption-Diffusion model for each replicate are reported in Table 2.
 553 The geometric impedance factor f (which controlled how long it took for P from the fertiliser granule
 554 to reach the probes) varied between 0.13 and 0.3, with most replicates requiring the default value
 555 0.3. The best-fit P-soil absorption rate (i.e. P removal from the soil solution due to multiple processes)
 556 $\tilde{\beta}_1$ was $1.1 \times 10^{-5} \text{ s}^{-1}$ for all replicates except L3, where the absorption rate was slightly reduced to
 557 capture the longer decay in the P2 probe phosphorus concentration measured in this experimental
 558 replicate, Figure 3F. Although we would expect the soil in all replicates to have the same P chemistry,
 559 heterogeneity of the soil can explain this result. The probe uptake rates, $\tilde{\delta}_{P1}$ and $\tilde{\delta}_{P2}$ varied the most
 560 between replicates to account for the probes with no or low P signals below the detection limit of the
 561 analytical method and the counter intuitive replicates where P2 had a higher concentration than P1.
 562 The Absorption-Diffusion model could characteristically capture the behaviour of the experimental
 563 probe measurements where fertiliser P was detected by the probe, *i.e.* E2, L1, L2 and L3, Figure 3 B,
 564 C, D, F. However, the model could not explain why the P2 probe measured a higher concentration of
 565 P, for example L2, Figure 3D.

566 *Table 2: Parameters in the Absorption-Diffusion model that best matched the microdialysis results. f is soil geometric*
 567 *impedance, $\tilde{\beta}_1$ is the effective adsorption rate of P, and $\tilde{\delta}_{Pi}$ are the probe P uptake rates.*

Replicate	f	$\tilde{\beta}_1$ [s^{-1}]	$\tilde{\delta}_{P1}$ [ms^{-1}]	$\tilde{\delta}_{P2}$ [ms^{-1}]
E1	0.3	1.1×10^{-5}	0	1×10^{-8}
E2	0.13	1.1×10^{-5}	2×10^{-8}	2×10^{-7}
E3	0.3	1.1×10^{-5}	5×10^{-10}	2×10^{-8}
L1	0.3	1.1×10^{-5}	2.94×10^{-8}	1.47×10^{-5}
L2	0.3	1.1×10^{-5}	1.5×10^{-8}	5×10^{-5}
L3	0.188	4×10^{-6}	2×10^{-9}	3×10^{-8}

568

569 Although the Absorption-Diffusion model did not perfectly capture the experimental probe
 570 measurements, it could capture characteristic features in the experiment that the Buffer Power model
 571 could not. When we used the Buffer Power model with buffer power $b=40$, the diffusion of P from the
 572 granule was too slow and the model probes did not detect it at all (Figure 4 A-B). If the buffer power
 573 was chosen as 1, then the P from the fertiliser granule reached the probes as it was not much slowed
 574 by chemical impedance, but the model probe measurement increased over time and did not decay
 575 like the experimental probe measurements (Figure 4 C-D). The decay in experimental probe P
 576 measurements was not likely to be caused by root uptake as we saw the same pattern in the non
 577 planted treatments (Figure S10). As further evidence that the roots cannot explain the decline in probe

578 P uptake we increased the root uptake by an order of magnitude ($F_p = 3.26 \times 10^{-7}$) in the Buffer
 579 Power model to see if this could result in a decay of the probe P flux. Even with enhanced root uptake,
 580 the Buffer Power model could not capture the decay in the experimental probe measurements (Figure
 581 4 E- F).

582

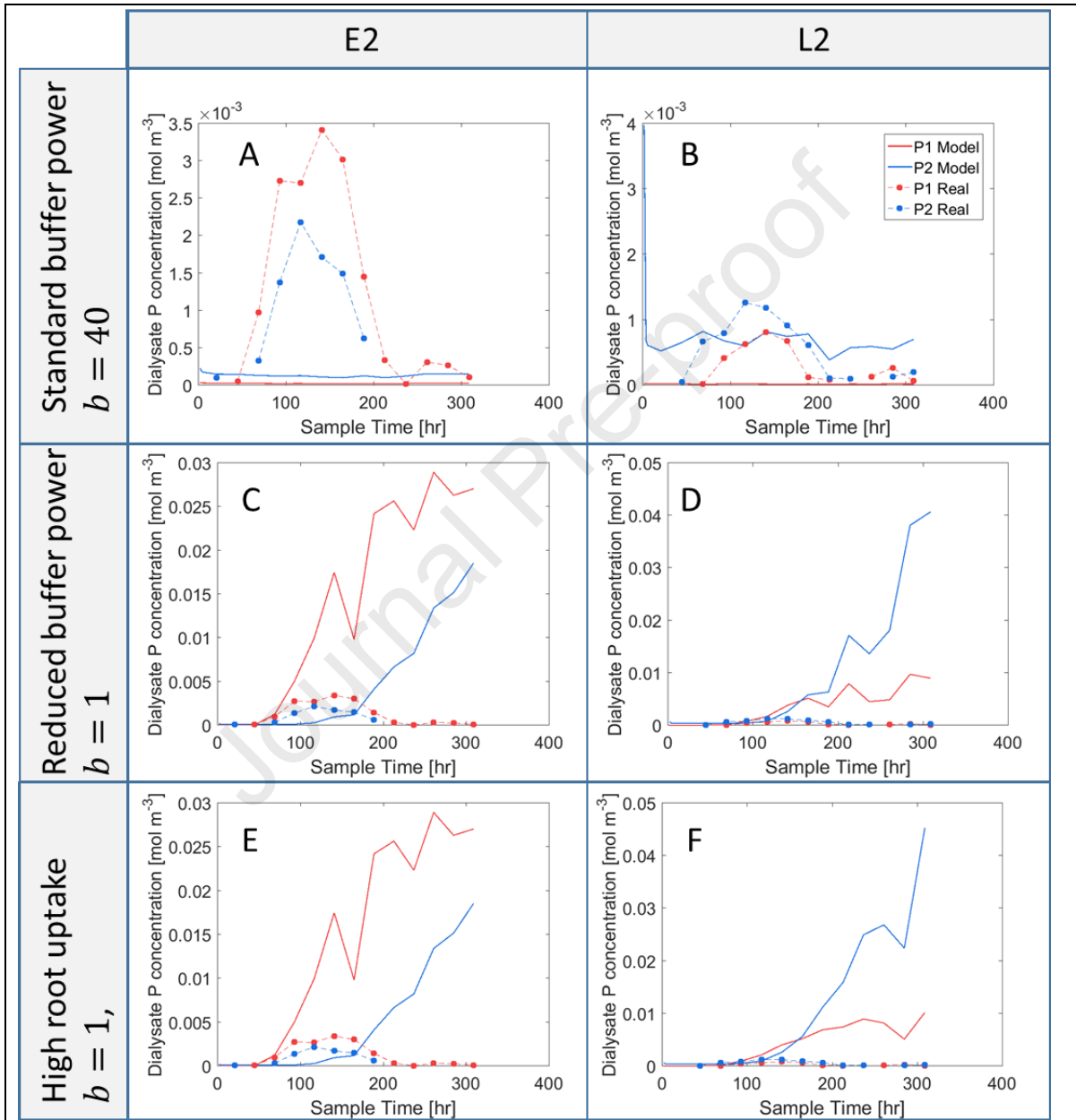


Figure 4: Experimental microdialysis results (dots + dashed lines) and comparison with Buffer Power model (solid lines) for two example replicates and a range of parameters. The figure demonstrates that the Buffer Power model does not capture the experimental system by showing both a typical and low buffer power selection does not characteristically match the experimental microdialysis results. Each model uses f , $\tilde{\delta}_{p1}$, and $\tilde{\delta}_{p2}$ as calculated from the data fitting performed by the

Absorption-Diffusion model while b and F_p vary. (A) E2 replicate, Buffer Power model with $b = 40$ and $F_p = 3.26 \times 10^{-8} \text{ mol m}^{-2} \text{ s}^{-1}$. (B) L2 replicate, Buffer Power model with $b = 40$ and $F_p = 3.26 \times 10^{-8} \text{ mol m}^{-2} \text{ s}^{-1}$. (C) E2 replicate, Buffer Power model with $b = 1$ and $F_p = 3.26 \times 10^{-8} \text{ mol m}^{-2} \text{ s}^{-1}$. (D) L2 replicate, Buffer Power model with $b = 1$ and $F_p = 3.26 \times 10^{-8} \text{ mol m}^{-2} \text{ s}^{-1}$. (E) E2 replicate, Buffer Power model with $b = 1$ and $F_p = 3.26 \times 10^{-7} \text{ mol m}^{-2} \text{ s}^{-1}$. (F) L2 replicate, Buffer Power model with $b = 1$ and $F_p = 3.26 \times 10^{-7} \text{ mol m}^{-2} \text{ s}^{-1}$.

583

584 4.4 Root uptake

585 In order to convert soil solution P concentrations to a biologically meaningful measurement, P uptake
 586 by the plants was measured both experimentally and numerically. Total elemental P concentrations
 587 were determined after total digestion of the plant biomass and are shown in Table 3. There was no
 588 significant difference in mean total P uptake between both fertilised treatments and un-fertilised
 589 (blank) treatment (two-sided student's t-test, $p > 0.05$). When considering above and below ground
 590 material separately the mean P concentrations of both early and late fertilised treatments are slightly
 591 higher than those of the blank, though not significantly. There was no significant difference in P uptake
 592 efficiency (total P uptake per unit root surface area) between the early, late and blank fertilisation
 593 treatments ($p > 0.05$).

594 *Table 3: Mean total P plant uptake and uptake efficiency as calculated from plant digestions at the end of the experiment.*
 595 *Above and below ground P concentration are the concentration in ppm in the above and below ground tissues. Total P is*
 596 *calculated as the sum of mean P concentration in the aboveground and belowground multiplied by their respective mass. P*
 597 *uptake efficiency is calculated as the total P divided by the replicates root surface area as calculated by the light microscopy*
 598 *images. Values show mean \pm standard deviation. Different lettered superscripts indicate significant differences as calculated*
 599 *from a two-sided student's t-test.*

	Early	Late	Blank
Above ground P concentration (ppm)	$7.8 \times 10^{-3} \pm 3 \times 10^{-2}$	$7.6 \times 10^{-3} \pm 3 \times 10^{-2}$	$6.3 \times 10^{-3} \pm 9 \times 10^{-2}$
Below ground P concentration (ppm)	$5.6 \times 10^{-3} \pm 1 \times 10^{-3}$	$5.4 \times 10^{-3} \pm 6 \times 10^{-2}$	$4.1 \times 10^{-3} \pm 7 \times 10^{-2}$
Total P uptake [mol]	$6.2 \times 10^{-5} \pm 2 \times 10^{-6a}$	$7.3 \times 10^{-5} \pm 7 \times 10^{-6a}$	$6.87 \times 10^{-5} \pm 1 \times 10^{-5a}$

P-uptake efficiency [mol m ⁻²]	$0.018 \pm 3 \times 10^{-3b}$	$0.014 \pm 3 \times 10^{-3b}$	$0.017 \pm 1 \times 10^{-3b}$
--	-------------------------------	-------------------------------	-------------------------------

600

601 To demonstrate the importance of accurately capturing the temporal availability of P from a fertiliser
 602 granule, the predicted root uptake dynamics for the two models are shown in Figure 5. The
 603 Absorption-Diffusion model predicted P concentration in the soil solution, thus readily available for
 604 root uptake, was only briefly enhanced by the fertiliser granule for approximately 8 – 13 days, Figure
 605 5A. The time (relative to planting) at which P uptake enhancement could happen is dependent on
 606 when the fertiliser was added and the time it takes for the P from the granule to dissolve and diffuse
 607 to the roots. In the early treatments the granule was added one week after planting and its effect on
 608 plant uptake is noticeable almost instantaneously, however, P uptake rate does not reach a peak until
 609 approximately 12 days after planting (*i.e.* 5 days after the addition of the fertiliser) Figure 5A. The
 610 enhanced P uptake was only brief and P uptake returned to its pre-fertiliser levels over 10 days. A
 611 similar trend can be observed for the late fertilisation replicates where the fertiliser granule was added
 612 49 days after planting, Figure 5A. In the late fertilisation replicates, the roots had more time to grow,
 613 hence we expected the roots to have more chance of taking up the P from the granule before it gets
 614 removed from the soil solution. However, this does not seem to be the case, as the root uptake in the
 615 late fertilisation is comparable to that of the early treatments (Figure 5A).

616 The Buffer Power model ($b = 40$) predicts a characteristically different root P uptake dynamics (Figure
 617 5B). In the early treatments, we can see a boost in P uptake as soon as the fertiliser is added to the
 618 soil at day 7. Unlike the Absorption-Diffusion model, P uptake rate continues to grow in the Buffer
 619 Power model as more P from the granule diffuses to the roots (Figure 5B). The initial peak in root
 620 uptake before the fertiliser has been added is due to the roots absorbing the P initially in soil, then the
 621 P adjacent to the roots becoming depleted due to slow diffusion resulting in a reduction in root uptake
 622 (Figure 5B).

623 Figure 6A shows the total P uptake for the Absorption-Diffusion (in red) and buffer power (in green)
 624 models, and the experimentally measured values (in grey). There was no significant difference
 625 between the treatments for the Absorption-Diffusion model. For the Buffer Power model, the early
 626 replicates have a significantly greater P uptake than the late replicates (one-sided students t-test,
 627 $p < 0.05$; Figure 6A) which is inconsistent with the experimental conclusions (Figure 6A).

628 Root P uptake efficiency (RUE) for both models and the experimental measurements is shown in Figure
 629 6B. The root surface area in the experimental measurements was calculated using the root washout

630 images while the models used the surface area extracted from the XCT scans. The mean of the early
 631 experimental root uptake efficiency is not significantly different from the late, (one-sided students t-
 632 test, $p > 0.05$, Figure 6B). The Absorption-Diffusion model correctly predicts no significant difference in
 633 uptake efficiency between the early and late treatments while the buffer model predicts a significant
 634 difference between early and late treatments with the early P uptake efficiency significantly higher
 635 than the late (one-sided students t-test, $p < 0.05$), Figure 6B, which is inconsistent with the
 636 experimental measurement.

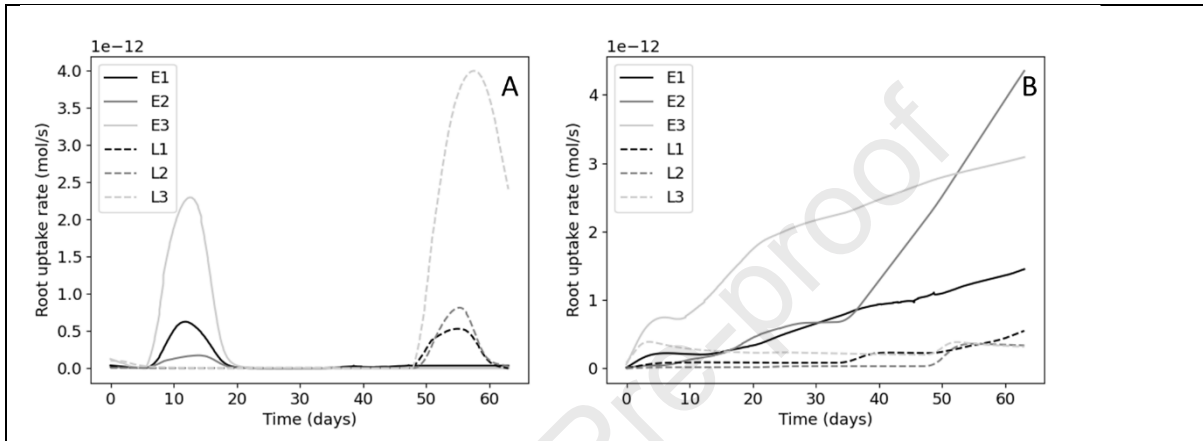


Figure 5: Comparison of modelled root uptake rates. Time in these plots are relative to planting date. (A) The root uptake rates as predicted by the Absorption-Diffusion model. Each replicate uses the parameters of best fit. (B) The root uptake rates as predicted by the Buffer Power model. Each model uses parameters f , $\tilde{\delta}_{p1}$ and $\tilde{\delta}_{p2}$ as calculated from the data fitting performed by the Absorption-Diffusion model and the buffer power $b = 40$.

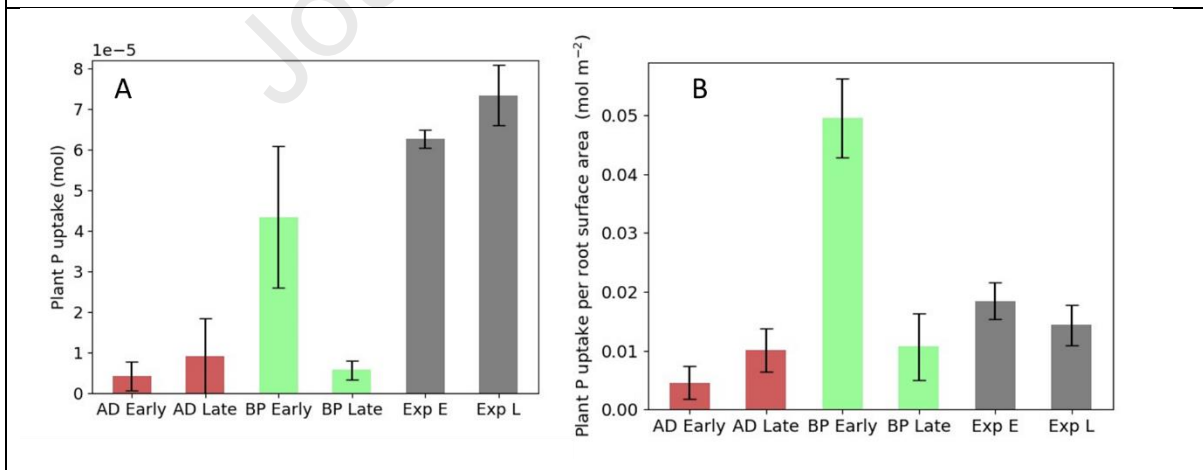


Figure 6: Mean total root uptake (A) and P uptake efficiency (B) of both models and the experimental measurement over early and late treatments. AD stands for Absorption-Diffusion model, BP stands for Buffer Power model, Exp stands for experimental value, E stands for early replicates and L stands for late replicates. Error bars show standard deviation. For the Absorption-Diffusion model, each replicate uses the parameters of best fit. For the Buffer Power model, each

model uses parameters f , $\tilde{\delta}_{P1}$ and $\tilde{\delta}_{P2}$ as calculated from the data fitting performed by the Absorption-Diffusion model and the buffer power is chosen $b = 40$. (A) Mean total root uptake. (B) Mean P uptake efficiency (Total P uptake per root surface area).

637 5. Discussion

638 In this study, we investigated the effects of different fertilisation regimes on soil solution P dynamics,
 639 plant root structure and growth, and we compared two different models to determine the most
 640 adequate to capture the observed dynamics. As seen in some previous studies, adding P fertiliser did
 641 not necessarily increase the growth of either the roots or shoots of the plants (Valkama et al., 2011;
 642 Macintosh et al., 2019). Here, we also did not find any increase in growth or proliferation of laterals
 643 close to the fertiliser granules, despite the use of low-STP soil and the fact that plant roots are known
 644 to proliferate in areas of locally high-STP. Not observing effects of the P treatment on plant growth
 645 could have multiple concurring causes: (i) added P is removed too quickly from the soil solution to be
 646 readily available to the plants; (ii) the plants grew using P reserves in the seed and did not grow long
 647 enough to reach the stage when they need to forage P from the surrounding soil; (iii) the alignment
 648 between the granules and the growing roots was not optimal to ensure P uptake in the narrow
 649 availability time window; (iv) plant growth was hindered by excessive soil moisture that was observed
 650 at the end of the experiment. In order to dynamically resolve the evolution of P concentration in the
 651 soil solution, we deployed microdialysis probes at various depths of our experimental soil column.
 652 Microdialysis results suggest that P is quickly released from the fertiliser granule to the soil solution
 653 (no chemical impedance) but is also quickly removed from solution in this low-STP soil (Figure 3), thus
 654 there is only a small time window when the added P from the granule is directly available to the plant
 655 roots in the soil solution. Matching this window with plant's needs can become important for precision
 656 agriculture practices. The microdialysis probes only detected P from the fertiliser in the soil solution
 657 for at most 8 days (Figure 3C), however, subsequent modelling suggests plants can only access the
 658 high concentrations of P in the soil solution for approximately 10 days starting straight after
 659 fertilisation (Figure 5A). This is due to the distribution of roots around the granule, which has to
 660 compete against the dynamic removal of P from the soil solution due to multiple processes such as
 661 sorption, precipitation and microbial activity. Over the short time-scale of the experiment P removed
 662 from the soil solution was not resolubilised, however, we expect the soil-retained P acts as 'Legacy-P'
 663 and can improve crop uptake in subsequent growing season (i.e. legacy P (Barrow, 1980)).

664 Data from the microdialysis measurements provided evidence for the need of a dynamic model
 665 capable of capturing the transport and retaining of P in a low-STP soil. This was demonstrated with an
 666 Absorption-Diffusion model, however, like all models, it is a simplification of a full kinetic processes

667 that cannot be observed with current technology. Although the model performed characteristically
668 similar to the measured results, there were certain features that could not be resolved by Absorption-
669 Diffusion model. Most notable was that in some cases the middle probe (P2) detected the pulse of P
670 from the granule earlier (E2, L2 and L3) and in higher quantities (L1, L2 and L3) than the probe closest
671 to the granule (Figure 3). It was unlikely this was due to the variation of the distances between the
672 probes and the granules, as shown in **Error! Reference source not found.** These counter intuitive
673 results could be explained by the probe uptake rate being affected by local environmental conditions,
674 or possibly, P moving by gravitational effects. It is possible that heavier P particles sink past the first
675 probe and dissolve in proximity of the P2 probe (Petroselli et al., 2021). We expect that this effect is
676 likely to be small as the soil is tortuous, and a large P particle is unlikely to sink far from the fertiliser
677 granule. Root exudation could generate locally enhanced zones of organic acid and low pH, which can
678 act to mobilise soil solid sorbed P (McKay Fletcher et al., 2020). Alternatively, root mucilage could also
679 play a role in reducing effective diffusivity in the soil pore space (Zarebanadkouki et al., 2019). These
680 features are not currently included in the model separately (they are included as a net effect), but it
681 seems at least one of these mechanisms plays a role in P transport from a fertiliser granule and should
682 be investigated in future studies.

683 However, the first improvements to the model should be the inclusion of the full first-order kinetics
684 (Barber, 1995) or the kinetic Langmuir reaction equation (Van de Weerd et al., 1999; Ruiz et al., 2021).
685 It is important to note that like the Buffer Power model, a Langmuir isotherm (Barber, 1995) would
686 not be able to capture the features seen in the microdialysis results. A Langmuir isotherm diffusion
687 model is a concentration dependent diffusion, with buffer power decreasing as concentration
688 increases. Thus, it would predict microdialysis probe uptake to be somewhere between the $b = 1$
689 and $b = 40$ (see Figure 4) for the Buffer Power model and not be able to capture the decay observed
690 using the experimental microdialysis probes (Figure 4). In the current study, it was not possible to
691 include full first-order kinetics (i.e. dynamics associated with desorption of P from the soil/minerals
692 into solution) due to the size and complexity of the domain needed to include root structure; first-
693 order kinetics requires the solution of the retained P equation, which requires additional memory, and
694 was thus not feasible with our computing systems. However, we can conclude that full soil-P dynamics,
695 be it Absorption-Diffusion, first order kinetics or non-linear kinetics like the Langmuir reactions, are
696 required to direct experimental observation of the P dissolution and transport from a fertiliser granule.

697 Any shortcomings of the Absorption-Diffusion model were also present in equilibrium reaction model
698 exemplified by the Buffer Power model here. The Buffer Power model was not satisfactory for
699 describing the experimental data. For a buffer power used to describe relatively mobile P in soils ($b =$
700 40), we found that the fertiliser P pulse was impeded so much that it never reached the probes (Figure

701 4 A and B). We reduced the buffer power to low values for P, which essentially emulates the situation
702 where all binding sites are occupied (*i.e.* high-STP soil and an extreme case of the Langmuir isotherm
703 model). We found that the pulse makes it to the probes. This resulted in a rise in the probe uptake
704 with no decay (Figure 4 C and D), which was inconsistent with the data. It was possible that the decay
705 in the experimental measurements was due to root uptake rather soil retaining. This is rejected due
706 to similar results in the non-planted treatment (see SM Figure S2). Additionally, we increased the
707 uptake by an order of magnitude, which likely breaks the kinetic limitations of the plant P uptake
708 (Barber, 1995). Despite this, the model was still not capable of reproducing the measurements (Figure
709 4 E and F). We note that in the previous study, we also found a similar decay behaviour within our
710 experiments, which did not include plant roots (Petroselli et al., 2021). It was clear that no
711 combination of buffer power, geometric impedance and probe uptake rates could achieve the
712 required decay in model probe concentration in the Buffer Power model or any equilibrium reaction
713 model. This result sheds light on some of the details of short-term processes that are often neglected
714 by long term and larger scale models and observation. We note that the soil conditions in this study
715 were low-STP (Olsen P = 12.6 mg L⁻¹)(AHDB, 2023) and that this soil has a high sorption capacity. We
716 attribute the poor performance of the Buffer Power model to reliance on the assumption that the
717 reaction rates are much faster than the diffusion timescale in its derivation (Barber, 1995; Roose et
718 al., 2001), and also note that the Langmuir isotherm diffusion model relies on this same assumption
719 (Van de Weerd et al., 1999; Ruiz et al., 2021). Since the buffer power for soils typically ranges from 40
720 to 1000, the absorption rate is orders of magnitude bigger than the desorption rate. In this study, we
721 demonstrated that the time scale for absorption was on the same order as the diffusion timescale,
722 which are both much more rapid than the dissolution timescale. Therefore, we did not find that
723 reaction equilibration was a suitable model for describing this experimental system.

724 We monitored the qualitative behaviour of root uptake in both models. The modelled plant uptake
725 simulated by the Absorption-Diffusion model demonstrates that most of the P is quickly removed from
726 the soil solution so only directly accessible to the plant for a brief period of time (Figure 5A). By
727 contrast, root uptake in the Buffer Power model remains constant until the fertiliser pulse reaches the
728 rooting zone. Then, in the early fertilisation scenario, the Buffer Power model exhibits an acceleration
729 in the root uptake (Figure 5B). This acceleration is caused by roots growing into P rich regions or P
730 from the fertiliser granule reaching further the roots. The late replicates with the Buffer Power model
731 did not achieve as high root uptake rates as the early replicates due to experimental cut-off times
732 prior to high P concentrations from the granule reaching the roots. It is worth highlighting that this is
733 a consequence of the time scale of the experiment.

734 We used the time integrated modelled root P uptake to compare the model results to the total P in
735 the experiments for the early and the late fertiliser application tests. For the early and late fertilisation
736 experiments, there were no significant differences between the total P content in the two treatments
737 (Figure 6A), however, the mean total P uptake in the late experiments was higher than in the early
738 ones. The experimental total P uptake was generally higher in magnitude by comparison to the
739 simulation results. Additionally, there was no significant difference in total P uptake between the
740 early, late, and no fertiliser experiments, suggesting P fertilisation could only marginally increase P
741 uptake. Differences for the results using the Absorption-Diffusion model, like the experimental results,
742 were not significant. However, the Absorption-Diffusion P uptake was lower in magnitude than the
743 experimentally measured values. By contrast to the Absorption-Diffusion model and the experimental
744 data, the Buffer Power model predicts early fertilisation would result in significantly more total P
745 uptake than the late. This would also imply that legacy-P would be lower for early fertilisation.

746 The Buffer Power model produced the incorrect conclusion regarding early and late fertilisation. The
747 no fertiliser control experiment alludes to the fact that the plants were unlikely to acquire significant
748 quantities of P from the fertiliser in the first 8 weeks from sowing and much of the measured total P
749 was likely already in the seed and soil from the beginning. The simulations only took into account P
750 taken up from the soil or fertiliser, which might explain why the Absorption-Diffusion model
751 underestimates the P by comparison to the experiments. It is also worth noting that the under-
752 prediction is also likely due to the model missing fine roots during segmentation or because the sixth
753 of the pot was not representative of the entire root system.

754 To try and account for the underrepresented roots, we compared the root uptake efficiency between
755 the three, *i.e.* experimental results, the Absorption-Diffusion model, and the Buffer Power model
756 (Figure 6B). Experimentally, the early tests had higher RUE values than the later tests, but the
757 differences were not significant. The Absorption-Diffusion model had slightly higher RUE in the late
758 treatments, but the difference was not significant. Lastly, the Buffer Power model had significantly
759 higher RUE in the early tests. In conclusion, the Buffer Power model appeared to be less in accordance
760 with the experimental data than the Absorption-Diffusion model. While the Absorption-Diffusion
761 model appears to be more representative of the actual experiments, there remain discrepancies
762 between the models and the experimental results in absolute value. These differences could be due
763 to the existence of dissolved P in the soil solution that is below the limits of detection of the analytical
764 method (Petroselli et al., 2021). In this case, the plants in the experiments have access to this low P
765 concentration that is not included in the Absorption-Diffusion model. Other soil P-processes that we
766 did not model which play a role in plant uptake and uptake efficiency could play an important role in
767 P uptake as discussed above. We attribute the poor performance of the equilibrium Buffer Power

768 model in estimating the root uptake in this study to the fact that the soil P was in a state of
769 disequilibrium due the addition of the fertiliser granule and the root uptake. However, agriculture soils
770 are often not in equilibrium (Nair, 2013) and our results demonstrate the importance of considering
771 kinetics.

Journal Pre-proof

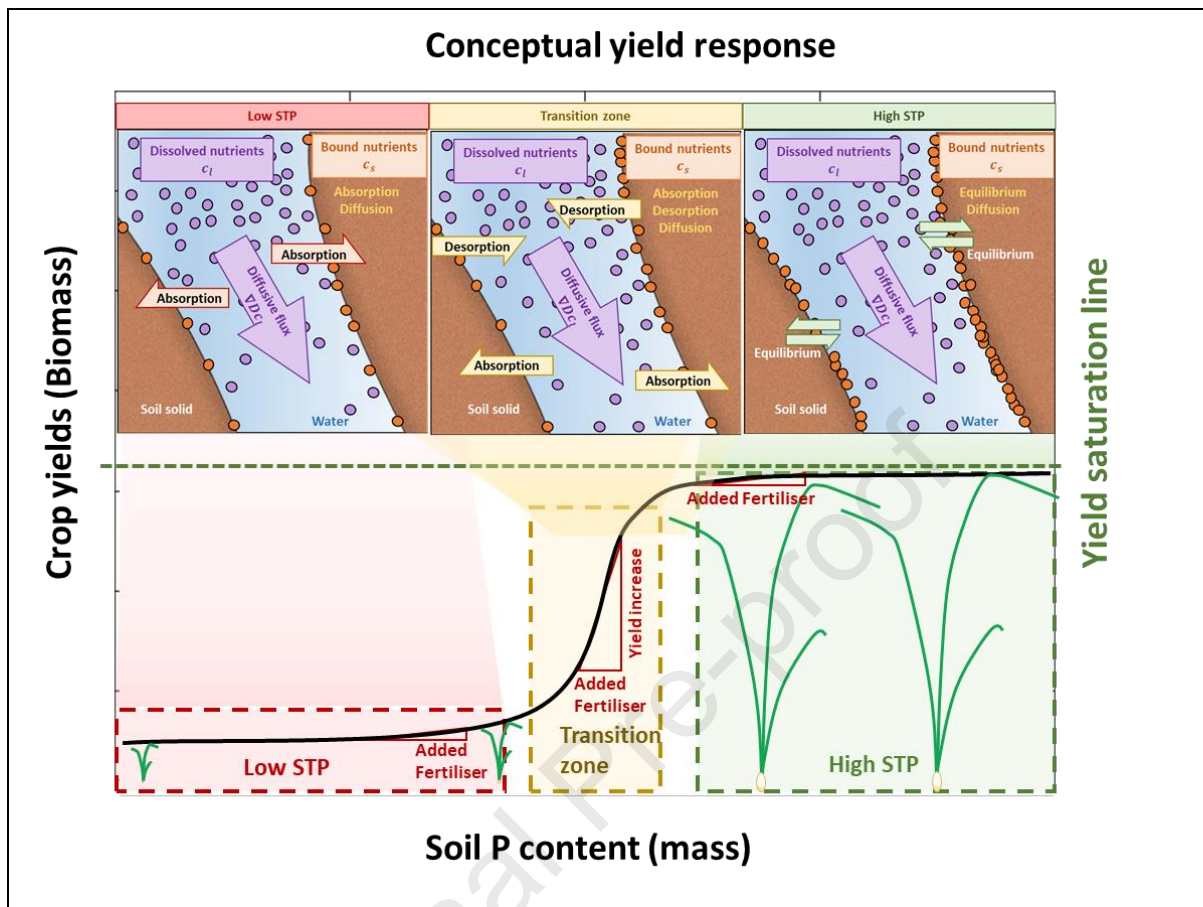


Figure 7: Conceptual model of crop yields as a function of soil P content. The current study was conducted on a low-STP soil, which required a dynamic Absorption-Diffusion model to characterise the soil P dynamics in a manner that was consistent with the microdialysis measurements. The results suggest that most of the added P fertiliser was rapidly removed from the soil solution before plants could directly access it. Literature studies on high-STP soils appear to demonstrate that there are diminishing returns on added fertilisation, and the systems can be readily modelled considering equilibrium reaction models. There is likely a transition zone where added fertilisation can result in increases in crop yields. We hypothesise that this transition zone would require a full soil type bespoke model that takes into consideration all of the absorption and desorption dynamics.

774 We can combine these findings together with previous literature to synthesise a general overview of
 775 soil P interactions and the resulting implications for crop yield enhancement over one growing season.
 776 From literature on soils with more readily available P (*i.e.* high-STP soils, Figure 7), it appears that
 777 applying fertiliser will likely provide minimal enhancement to crop yields that year (Valkama et al.,
 778 2011; Macintosh et al., 2019). Under high-STP conditions, once P is removed from the soil solution by
 779 the roots, it is replenished by the soil (Rowe et al., 2016). Utilizing this 'legacy P' in high-STP soils is

780 vital for reducing our dependence on rock phosphate and sustainable agriculture (Rowe et al., 2016).
781 Under these conditions, there are diminishing returns on additional P fertilisation in the form of yields
782 (Figure 7) and P fertilisation comes with risk of leaching and runoff (Fischer et al., 2017; Macintosh et
783 al., 2019). In these scenarios we predict an equilibrium reaction model would be suitable for capturing
784 this scenario since desorption happens faster than in the low-STP case.

785 Our experiments were conducted on a low-STP soil and we saw negligible increase in plant P uptake
786 with P fertilisation (Table 3) thus we deem in these conditions there would be little yield response
787 with this level of fertilisation as conceptually displayed in Figure 7. There is evidence of poor yield
788 response to P fertilisation in low and medium STP soils, see field trials of (Valkama et al., 2011) for
789 example. Additionally, it is implied with the common use of the Langmuir isotherm where the
790 proportion of plant-available P increases with total P (Barber, 1995). However, with this model one
791 would expect higher P uptake with fertilisation. It is important to note that the experimental
792 conditions only lasted 9 weeks and were not representative of an entire growing season. It could be
793 the case that the crop could utilize the sorbed P over the growing season. However, early P uptake is
794 important for yield (Talboys et al., 2016) and the poor early P uptake in this experiment would have
795 cumulative effect for subsequent yield, regardless of later P utilization. The microdialysis probes
796 determined that the poor P uptake seen in the plant digestions was due to only a brief window
797 (approximately 5-8 days) of enhanced solution P availability (Figure 3). Modelling suggests that this
798 brief window only lasts for approximately 10 days (Figure 5). There seems to be two options for
799 improving P uptake and thus yield in low-STP soils with P fertilisation. First, apply large quantities of P
800 to saturate the soil P binding sites and get to the rapidly increasing point on the curve shown in Figure
801 7. It is possible this could take a number of years. However, this approach is expensive and carries the
802 risk of nutrient leaching and run-off (Fischer et al., 2017).

803 Alternatively, precision agriculture techniques (Cisternas et al., 2020) in combination with plant
804 breeding could be used to make the most of the brief window of enhanced P uptake. This might be
805 achieved through a few different avenues. For example, precision placement of the fertiliser to ensure
806 maximal root proximity, or timing the application with rainfall and soil moisture to control the pulse
807 of available P from the fertiliser granule. Results suggest that when sampling the soil for precision
808 agriculture techniques, the brief time-window of P availability in the soil solution should be taken into
809 consideration. Plant traits such as the exudation of organic acids could help the plant solubilise
810 retained P after the initial pulse (Jones, 1998; Gerke et al., 2000). Thus breeding and using high exuding
811 varieties (McGrail et al., 2021) could improve P uptake in the current conditions. To test the role
812 organic acids in P acquisition from a fertiliser granule in these conditions, we recommend using the
813 current experimental setup, but infusing the microdialysis probes with organic acids which exude into

814 the soil while simultaneously sampling soil solution P (Demand et al., 2017; McKay Fletcher et al.,
815 2019).

816 It appears that when adding P fertiliser granules to a low-STP soil, roots will be in competition with
817 the soil to take up the pulse of solution P from the fertiliser – a feature that is not accounted for when
818 using equilibrium models like the Buffer Power model. Furthermore, neither early nor late fertilisation
819 will make a difference on these time scales. In these conditions it is important to make use of plant
820 strategies for solubilising and harvesting retained P (Wen et al., 2019). From previous literature it is
821 clear adding fertilisers to a high-STP soil will not provide any benefit, as there is likely abundant P for
822 plant use. However, there is likely to be a regime between low-STP and high-STP where there will be
823 a good yield response to fertilisation (Figure 7), but this would be very soil type dependent. Within
824 this regime, neither of the models used in this study will likely be adequate for describing the dynamics
825 of the system. To properly estimate the gains in this regime, the full model (eq. **Error! Reference**
826 **source not found.**) will likely need to be invoked.

827 Understanding how soil P dynamics in low-STP and high-STP regimes can curb larger scale P deficits
828 through enhancing fertiliser use efficiency, which will aid in larger sustainable practices (Cordell et al.,
829 2009). For example, arable land in the UK makes up over 3×10^6 ha of land. Assuming that there's an
830 accumulation rate of $5.7 \text{ kg ha}^{-1} \text{ yr}^{-1}$ (estimated by the 700 kg ha^{-1} accumulation in the EU since 1900
831 (Kahiluoto et al., 2021)) and the cost of P fertilisers is at $0.320 \text{ EUR kg}^{-1}$ (Mundi, 2022), this means that
832 the UK can be saving over 5M EUR annually through efficient P allocation. Moreover, identifying the
833 transition zone between low-STP to high-STP soils will also help in planning sensible fertilisation
834 strategies. Finally, future studies will have to identify the nuanced dynamics that take place during the
835 transition between high-STP to low-STP in order to avoid future losses considering the current volatile
836 prices for P (Mundi, 2022).

837

838 Acknowledgements and funding statements

839 The authors would like to acknowledge the μ -VIS X-ray Imaging Centre at the University of
840 Southampton for provision of tomographic imaging facilities, and in particular Dr. Sebastian Rosini and
841 Dr. Kathryn Rankin for their valuable support with the XCT scans. C.P, S.A.R., K.A.W, D.M.F. and T.R.
842 are funded by ERC Consolidator grant 646809 (Data Intensive Modelling of the Rhizosphere
843 Processes). T.R. is also funded by, BBSRC SARIC BB/P004180/1, BBSRC SARISA BB/L025620/1 and
844 EPSRC EP/M020355/1. S.A.R is also funded by BBSRC Discovery Fellowship BB/X010147/1 and Royal

845 Society University Research Fellowship URF\R1\231622. D.M.F: This work was supported by the Rural
846 and Environment Science and Analytical Services Division (SRUC-C5-1).

847

848 Competing interests statement

849 The authors declare no conflict of interests.

850 Author contributions

851 Conceptualization (CP, KW, TR); Data curation (CP, KW); Mathematical modelling (SR, DMF);
852 Interpretation (SR,DMF); Formal analysis (CP, KW, SR, DMF); Funding acquisition (TR); Investigation
853 (CP, KW, SR, DMF); Methodology (CP, KW, SR, DMF, MJC); Project administration (TR); Resources
854 (TR); Supervision (TR); Validation (CP, KW, SR, DMF, MJC); Visualization (CP, KW, SR, DMF); Writing –
855 original draft (CP, KW, SR, DMF); Writing – review and editing (CP, KW, SR, DMF, MJC, TR).

856 References

- 857 AHDB, U., 2023. Nutrient management guide (RB209). AHDB Warwickshire, UK.
- 858 Ahmed, S., Klassen, T.N., Keyes, S., Daly, M., Jones, D.L., Mavrogordato, M., Sinclair, I., Roose, T., 2016.
- 859 Imaging the interaction of roots and phosphate fertiliser granules using 4D X-ray tomography. *Plant*
- 860 *and Soil* 401, 125-134.
- 861 Barber, S.A., 1995. Soil nutrient bioavailability: a mechanistic approach. John Wiley & Sons.
- 862 Barrow, N., 1974. The slow reactions between soil and anions: 1. Effects of time, temperature, and
- 863 water content of a soil on the decrease in effectiveness of phosphate for plant growth. *Soil Science*
- 864 118, 380-386.
- 865 Barrow, N., 1980. Evaluation and utilization of residual phosphorus in soils. The role of phosphorus in
- 866 agriculture, 333-359.
- 867 Barrow, N., 1983. A mechanistic model for describing the sorption and desorption of phosphate by
- 868 soil. *Journal of Soil Science* 34, 733-750.
- 869 Benbi, D., Gilkes, R., 1987. The movement into soil of P from superphosphate grains and its availability
- 870 to plants. *Fertilizer Research* 12, 21-36.
- 871 Bolland, M.D., Gilkes, R.J., 1998. The chemistry and agronomic effectiveness of phosphate fertilizers.
- 872 *Journal of Crop Production* 1, 139-163.
- 873 Buckley, S., Brackin, R., Jämtgård, S., Näsholm, T., Schmidt, S., 2020. Microdialysis in soil environments:
- 874 Current practice and future perspectives. *Soil Biology and Biochemistry* 143, 107743.
- 875 Cisternas, I., Velásquez, I., Caro, A., Rodríguez, A., 2020. Systematic literature review of
- 876 implementations of precision agriculture. *Computers and Electronics in Agriculture* 176, 105626.
- 877 Condon, L.M., Turner, B.L., Cade-Menun, B.J., 2005. Chemistry and dynamics of soil organic
- 878 phosphorus. *Phosphorus: agriculture and the environment* 46, 87-121.
- 879 Cordell, D., Drangert, J.-O., White, S., 2009. The story of phosphorus: global food security and food for
- 880 thought. *Global environmental change* 19, 292-305.
- 881 Cornish, P.S., 2009. Research directions: Improving plant uptake of soil phosphorus, and reducing
- 882 dependency on input of phosphorus fertiliser. *Crop and Pasture Science* 60, 190-196.
- 883 Demand, D., Schack-Kirchner, H., Lang, F., 2017. Assessment of diffusive phosphate supply in soils by
- 884 microdialysis. *Journal of Plant Nutrition and Soil Science*.
- 885 Doube, M., Kłosowski, M.M., Arganda-Carreras, I., Cordelières, F.P., Dougherty, R.P., Jackson, J.S.,
- 886 Schmid, B., Hutchinson, J.R., Shefelbine, S.J., 2010. BoneJ: Free and extensible bone image analysis in
- 887 ImageJ. *Bone* 47, 1076-1079.
- 888 Fischer, P., Pöthig, R., Venohr, M., 2017. The degree of phosphorus saturation of agricultural soils in
- 889 Germany: Current and future risk of diffuse P loss and implications for soil P management in Europe.
- 890 *Science of the total environment* 599, 1130-1139.
- 891 Gao, W., Blaser, S.R., Schlüter, S., Shen, J., Vetterlein, D., 2019a. Effect of localised phosphorus
- 892 application on root growth and soil nutrient dynamics in situ—comparison of maize (*Zea mays*) and
- 893 faba bean (*Vicia faba*) at the seedling stage. *Plant and Soil* 441, 469-483.
- 894 Gao, W., Schlüter, S., Blaser, S.R., Shen, J., Vetterlein, D., 2019b. A shape-based method for automatic
- 895 and rapid segmentation of roots in soil from X-ray computed tomography images: Routine. *Plant and*
- 896 *Soil* 441, 643-655.
- 897 Gerke, J., Beißner, L., Römer, W., 2000. The quantitative effect of chemical phosphate mobilization by
- 898 carboxylate anions on P uptake by a single root. I. The basic concept and determination of soil
- 899 parameters. *Journal of Plant Nutrition and Soil Science* 163, 207-212.
- 900 Hammarlund-Udenaes, M., 2017. Microdialysis as an important technique in systems pharmacology—
- 901 a historical and methodological review. *The AAPS journal* 19, 1294-1303.
- 902 Hedley, M., McLaughlin, M., 2005. Reactions of phosphate fertilizers and by-products in soils.
- 903 *Phosphorus: agriculture and the environment* 46, 181-252.
- 904 Hoagland, D.R., Arnon, D.I., 1950. The water-culture method for growing plants without soil. *Circular*.
- 905 *California agricultural experiment station* 347.

- 906 Jones, D.L., 1998. Organic acids in the rhizosphere—a critical review. *Plant and Soil* 205, 25-44.
- 907 Kahiluoto, H., Pickett, K.E., Steffen, W., 2021. Global nutrient equity for people and the planet. *Nature*
- 908 *Food* 2, 857-861.
- 909 König, A., Wiesenbauer, J., Gorka, S., Marchand, L., Kitzler, B., Inselsbacher, E., Kaiser, C., 2022.
- 910 Reverse microdialysis: A window into root exudation hotspots. *Soil Biology and Biochemistry* 174,
- 911 108829.
- 912 Macintosh, K.A., Doody, D.G., Withers, P.J., McDowell, R.W., Smith, D.R., Johnson, L.T., Bruulsema,
- 913 T.W., O'Flaherty, V., McGrath, J.W., 2019. Transforming soil phosphorus fertility management
- 914 strategies to support the delivery of multiple ecosystem services from agricultural systems. *Science of*
- 915 *the total environment* 649, 90-98.
- 916 McGrail, R.K., Van Sanford, D.A., McNear Jr, D.H., 2021. Semidwarf winter wheat roots contain fewer
- 917 organic acids than wild-type varieties under phosphorus stress. *Crop Science* 61, 3586-3597.
- 918 McKay Fletcher, D., Shaw, R., Sánchez-Rodríguez, A., Daly, K., Van Veelen, A., Jones, D., Roose, T.,
- 919 2019. Quantifying citrate-enhanced phosphate root uptake using microdialysis. *Plant and Soil*, 1-21.
- 920 McKay Fletcher, D.M., Ruiz, S., Dias, T., Petroselli, C., Roose, T., 2020. Linking root structure to
- 921 functionality: the impact of root system architecture on citrate-enhanced phosphate uptake. *New*
- 922 *Phytologist* 227, 376-391.
- 923 Mundi, I., 2022. Rock phosphate monthly price—Euro per metric ton.
- 924 Nair, K.P., 2013. The buffer power concept and its relevance in African and Asian soils. *Advances in*
- 925 *Agronomy* 121, 447-516.
- 926 Nziguheba, G., Zingore, S., Kihara, J., Merckx, R., Njoroge, S., Otinga, A., Vandamme, E., Vanlauwe, B.,
- 927 2016. Phosphorus in smallholder farming systems of sub-Saharan Africa: implications for agricultural
- 928 intensification. *Nutrient Cycling in Agroecosystems* 104, 321-340.
- 929 Oburger, E., Jones, D.L., Wenzel, W.W., 2011. Phosphorus saturation and pH differentially regulate the
- 930 efficiency of organic acid anion-mediated P solubilization mechanisms in soil. *Plant and Soil* 341, 363-
- 931 382.
- 932 Oburger, E., Kirk, G.J., Wenzel, W.W., Puschenreiter, M., Jones, D.L., 2009. Interactive effects of
- 933 organic acids in the rhizosphere. *Soil Biology and Biochemistry* 41, 449-457.
- 934 Petroselli, C., Williams, K.A., Ghosh, A., McKay Fletcher, D., Ruiz, S.A., Gerheim Souza Dias, T., Scotson,
- 935 C.P., Roose, T., 2021. Space and time-resolved monitoring of phosphorus release from a fertilizer pellet
- 936 and its mobility in soil using microdialysis and X-ray computed tomography. *Soil Science Society of*
- 937 *America Journal* 85, 172-183.
- 938 Pierzynski, G.M., McDowell, R.W., Thomas Sims, J., 2005. Chemistry, cycling, and potential movement
- 939 of inorganic phosphorus in soils. *Phosphorus: agriculture and the environment* 46, 51-86.
- 940 Roose, T., Fowler, A., Darrah, P., 2001. A mathematical model of plant nutrient uptake. *Journal of*
- 941 *mathematical biology* 42, 347-360.
- 942 Ros, M.B., Koopmans, G.F., van Groenigen, K.J., Abalos, D., Oenema, O., Vos, H.M., van Groenigen,
- 943 J.W., 2020. Towards optimal use of phosphorus fertiliser. *Scientific reports* 10, 1-8.
- 944 Rowe, H., Withers, P.J., Baas, P., Chan, N.I., Doody, D., Holiman, J., Jacobs, B., Li, H., MacDonald, G.K.,
- 945 McDowell, R., 2016. Integrating legacy soil phosphorus into sustainable nutrient management
- 946 strategies for future food, bioenergy and water security. *Nutrient Cycling in Agroecosystems* 104, 393-
- 947 412.
- 948 Rueden, C.T., Schindelin, J., Hiner, M.C., DeZonia, B.E., Walter, A.E., Arena, E.T., Eliceiri, K.W., 2017.
- 949 ImageJ2: ImageJ for the next generation of scientific image data. *BMC bioinformatics* 18, 529.
- 950 Ruiz, S., McKay Fletcher, D., Williams, K., Roose, T., 2021. Plant–soil modelling. *Annu. Plant Rev. Online*
- 951 4, 127-198.
- 952 Sattari, S., Van Ittersum, M., Giller, K., Zhang, F., Bouwman, A., 2014. Key role of China and its
- 953 agriculture in global sustainable phosphorus management. *Environmental Research Letters* 9, 054003.
- 954 Sattari, S.Z., Bouwman, A.F., Giller, K.E., van Ittersum, M.K., 2012. Residual soil phosphorus as the
- 955 missing piece in the global phosphorus crisis puzzle. *Proceedings of the National Academy of Sciences*
- 956 109, 6348-6353.

- 957 Schachtman, D.P., Reid, R.J., Ayling, S.M., 1998. Phosphorus uptake by plants: from soil to cell. *Plant*
958 *physiology* 116, 447-453.
- 959 Schindelin, J., Arganda-Carreras, I., Frise, E., Kaynig, V., Longair, M., Pietzsch, T., Preibisch, S., Rueden,
960 C., Saalfeld, S., Schmid, B., 2012. Fiji: an open-source platform for biological-image analysis. *Nature*
961 *methods* 9, 676-682.
- 962 Schnepf, A., Leitner, D., Klepsch, S., 2012. Modeling phosphorus uptake by a growing and exuding root
963 system. *Vadose Zone Journal* 11.
- 964 Talboys, P.J., Heppell, J., Roose, T., Healey, J.R., Jones, D.L., Withers, P.J., 2016. Struvite: a slow-release
965 fertiliser for sustainable phosphorus management? *Plant and Soil* 401, 109-123.
- 966 Tinker, P.B., Nye, P.H., 2000. *Solute movement in the rhizosphere*. Oxford University Press.
- 967 Valkama, E., Uusitalo, R., Turtola, E., 2011. Yield response models to phosphorus application: a
968 research synthesis of Finnish field trials to optimize fertilizer P use of cereals. *Nutrient Cycling in*
969 *Agroecosystems* 91, 1-15.
- 970 Van de Weerd, H., Van Riemsdijk, W., Leijnse, A., 1999. Modeling the dynamic adsorption/desorption
971 of a NOM mixture: Effects of physical and chemical heterogeneity. *Environmental Science &*
972 *Technology* 33, 1675-1681.
- 973 VanRossum, G., Drake, F.L., 2010. *The python language reference*. Python Software Foundation
974 Amsterdam, Netherlands.
- 975 Wen, Z., Li, H., Shen, Q., Tang, X., Xiong, C., Li, H., Pang, J., Ryan, M.H., Lambers, H., Shen, J., 2019.
976 Tradeoffs among root morphology, exudation and mycorrhizal symbioses for phosphorus-acquisition
977 strategies of 16 crop species. *New Phytologist* 223, 882-895.
- 978 Williams, K., McKay Fletcher, D., Petroselli, C., Ruiz, S., Roose, T., 2022. A 3D image-based modelling
979 approach for understanding spatiotemporal processes in phosphorus fertiliser dissolution, soil
980 buffering and uptake by plant roots. *Scientific reports* 12, 1-13.
- 981 Zarebanadkouki, M., Fink, T., Benard, P., Banfield, C.C., 2019. Mucilage facilitates nutrient diffusion in
982 the drying rhizosphere. *Vadose Zone Journal* 18, 1-13.
- 983

Highlights

1. Phosphorus fertiliser dynamics and inefficiency sources are poorly understood
2. We investigated spatiotemporal dynamics of P in soil and plant uptake
3. We combined microdialysis, X-ray Computed Tomography and image-based modelling
4. Explaining rapid P adsorption in P-poor soil required a novel modelling approach
5. New models predict P application is effective in a narrow window of P-soil content

Journal Pre-proof

Declaration of interests

The authors declare that they have no known competing financial interests or personal relationships that could have appeared to influence the work reported in this paper.

The authors declare the following financial interests/personal relationships which may be considered as potential competing interests:

Journal Pre-proof